 doi:10.20944/preprints202104.0026.v1

Type of the Paper (Article, Review, Communication, etc.)

Triphenilphosphonium analogs of chloramphenicol as dual-acting antimicrobial and antiproliferating agents

Julia A. Pavlova[1], Zimfira Z. Khairullina[1], Andrey G. Tereshchenkov[2], Pavel A. Nazarov[2,3], Dmitrii A. Lukianov[4], Inna A. Volynkina[5], Dmitry A. Skvortsov[1], Gennady I. Makarov[6], Etna Abad[7], Somay Y. Murayama[8], Susumu Kajiwara[9], Alena Paleskava[10,11], Andrey L. Konevega[10,11,12], Yuri N. Antonenko[2], Alex Lyakhovich[13,14], Ilya A. Osterman[1,4,#], Alexey A. Bogdanov[1,2], and Natalia V. Sumbatyan[1,2,#]

[1] Lomonosov Moscow State University, Department of Chemistry, Leninskie Gory, 1, bldg 3, 119991 Moscow, Russia
[2] Lomonosov Moscow State University, A.N. Belozersky Institute of Physico-Chemical Biology, Leninskie Gory, 1, bldg 40, 119992 Moscow, Russia
[3] Laboratory of Molecular Genetics, Moscow Institute of Physics and Technology, Moscow Region, 141700 Dolgoprudny, Russia
[4] Center of Life Sciences, Skolkovo Institute of Science and Technology, Skolkovo, 143028 Russia
[5] School of Bioengineering and Bioinformatics, Lomonosov Moscow State University, Moscow 119992, Russia
[6] South Ural State University, 454080 Chelyabinsk, Russia
[7] Department of Experimental and Health Sciences, Universitat Pompeu Fabra, Barcelona, Spain
[8] Laboratory of Molecular Cell Biology, School of Pharmacy, Nihon University, Funabashi, Chiba 274-8555, Japan.
[9] School of Life Science and Technology, Tokyo Institute of Technology, Yokohama, Kanagawa 226-8501, Japan
[10] Petersburg Nuclear Physics Institute, NRC "Kurchatov Institute", Gatchina, 188300, Russia
[11] Peter the Great St.Petersburg Polytechnic University, Saint Petersburg, 195251, Russia
[12] NRC "Kurchatov Institute", Moscow, 123182, Russia
[13] Institute of Molecular Biology and Biophysics, Federal Research Center of Fundamental and Translational Medicine, Novosibirsk, Russia
[14] Vall D'Hebron Institut de Recerca, 08035, Barcelona, Spain
Correspondence: sumbtyan@belozersky.msu.ru (N.V.S.); i.osterman@skoltech.ru (I.A.O.)

Abstract: In the current work, in continuation of our recent research [1] we synthesized and studied new chimeric compounds comprising the ribosome-targeting antibiotic chloramphenicol (CHL) and the membrane-penetrating cation triphenylphosphonium (TPP) connected by alkyl linkers of different lengths. Using various biochemical assays, we showed that these CAM-Cn-TPP compounds bind to the bacterial ribosome, inhibit protein synthesis *in vitro* and *in vivo* in a way similar to that of the parent CHL, and significantly decrease membrane potential. Similar to CAM-C4-TPP, the mode of action of CAM-C10-TPP and CAM-C14-TPP on bacterial ribosomes differ from that of CHL. By simulating the dynamics of complexes of CAM-Cn-TPP with bacterial ribosomes, we have proposed a possible explanation for the specificity of the action of these analogs on the translation process. CAM-C10-TPP and CAM-C14-TPP stronger inhibit the growth of the Gram-positive bacteria in comparison to the CHL and suppress some strains of CHL-resistant bacteria. Thus, we have shown that TPP derivatives of CHL are dual-acting compounds that target the ribosomes and the cellular membranes of bacteria. The TPP fragment of CAM-Cn-TPP compounds contributes to the inhibitory effect on bacteria. Moreover, since the mitochondria of eukaryotic cells have qualities similar to those of their prokaryotic ancestors, we demonstrate the possibility of targeting chemoresistant cancer cells with these compounds.

Keywords: chloramphenicol; alkyl(triphenyl)phosphonium; bacterial ribosome; molecular dynamics simulations; antibiotic activity; antiproliferative activity

Research highlights

- Similar to the parent CHL, CAM-C10-TPP and CAM-C14-TPP bind to the 70S ribosome and specifically inhibit protein synthesis *in vitro* as well as in bacterial cells;

 doi:10.20944/preprints202104.0026.v1

- Introduction of TPP moiety in the structures of CHL analogs results in significant decreasing of membrane potential on bacterial cells;
- TPP derivatives of CHL (CAM-C10-TPP and CAM-C14-TPP) more strongly inhibit the growth of Gram-positive bacteria in comparison to the parent CHL and suppress some strains of CHL resistant bacteria;
- The TPP derivative of CHL exhibits an antimicrobial effect acting simultaneously on ribosomes and bacterial membranes.
- TPP-derivatives can target mitochondria in chemoresistant breast cancer cells and derived cancer stem-like cells and reduce their proliferation.

 doi:10.20944/preprints202104.0026.v1

1. Introduction

The search for new antimicrobial agents remains a crucial and urgent need, largely due to the existence and never-ending emergence of resistant bacterial strains that have various mechanisms of acquired resistance to nearly all clinically relevant antibiotics. These mechanisms include mutations in the drug target site, enzymatic modification or degradation of antibiotics, active efflux through porins, and other permeability barriers [2, 3, 4].

One of the promising approaches to creating new antibiotics is to design the so-called twin-drugs – dual-acting compounds containing two pharmacophores that are covalently linked in the same molecule. This approach allows to potentially create drugs that are active against drug-resistant microorganisms, have an expanded spectrum of antibacterial activity compared with the original antibiotics, and have a reduced potential for generation of bacterial resistance [5]. While each of the two pharmacophores in such a hybrid drug molecule is expected to act independently upon its original biological target, the non-cleavable covalent linker tethering the two active moieties endows the drug with a dual mechanism of action. These pharmacophores can be either two antibiotics or an antibiotic with an adjuvant that increases the access of the drug to its intracellular target (e.g., an efflux pump inhibitor or membrane and cell wall penetrating group or a moiety changing the physical properties of the molecule).

Quinolone-based hybrid compounds, especially fluoroquinolones associated with other antibacterial agents, such as oxazolidinones, anilinouracil compounds, tetracyclines, benzylpyrimidine, macrolides, quinolones, oxoquinolysines, or aminoglycosides, are the best-studied examples of the tethered antibiotics [6, 7, 8]. Many studies on the development of dual-acting compounds have been conducted on aminoglycosides by linking these molecules to quinolones, as well as to β-lactam antibiotics, CHL, oxazolidinones, or short amphiphilic peptides. Some dual-acting antibiotics comprising glycopeptides have been synthesized to include β-lactam, macrolide moieties, or fragments of natural antimicrobial peptides [7, 8, 9]. Many of these compounds exhibited high antibacterial activity not only against Gram-positive strains but also against Gram-negative bacteria, have a broad spectrum of activity and reduced toxicity to the mammalian host compared to the original antibiotics, and were also active against bacterial drug-resistant strains. A number of such hybrid antibiotics had clinical success over the past years [8].

Another type of dual-acting antibiotics are hybrid compounds containing a component that inhibits the efflux pumps, whose mutations are the main cause of intrinsic resistance to antibiotics currently available against Gram-negative bacteria. This component can be either non-antibacterial [10, 11, 8] or antibacterial [7, 8, 12]. For example, aminoquinolones or tobramycin have been used for constructing dual-acting agents not only as antibiotics but also as inhibitors of membrane efflux pumps [12].

Another kind of molecules that can be used in the design of dual-acting antibiotics are moieties that provide better penetration of the antibiotic into bacterial cells. For example, siderophores, which are high-affinity iron chelators produced by bacteria and fungi, have been successfully used in the past to aid the active transport of antibiotics into bacterial cells to enhance the action of β-lactam or penicillin antibiotics [8, 12]. Moreover, benzoxaboroles are known to enhance the transport of macromolecules into the cell as a result of interaction with 1,2- and 1,3-diol polysaccharides located on the cell surface. These properties, as well as the ability of some heterocyclic boronic acids and benzoxaborole derivatives to exhibit activity against Gram-negative bacteria with multi-drug resistance, were considered in the development of chimeric antibiotics based on glycopeptides or polyene macrocyclic antibiotics containing benzoxaboroles in their structure [7, 13] as well as benzoxaborole derivatives of azithromycin [9].

Triphenylphosphonium (TPP) is a synthetic cation that readily penetrates biological membranes. The positive charge of this moiety is scattered over the three phenyl resi-

 doi:10.20944/preprints202104.0026.v1

dues. As a result, the water dipoles cannot be retained by the cation and, thus, do not form an aqueous shell preventing the ion from penetrating the membrane using the energy of the transmembrane potential [14]. TPP and its synthetic derivatives have been actively studied mainly as mitochondria-targeting compounds, revealing many interesting properties that can be used to create therapeutic agents [15, 16]. In particular, alkyl-TPPs and their derivatives exhibit properties of mild uncouplers of oxidative phosphorylation, with a mechanism comprising the interaction of alkyl-TPP cations with anions of fatty acids, facilitating fatty acid cycling in the membrane [17]. It has also been shown that TPP derivatives exhibit antibacterial properties [18, 19, 20, 21, 22, 23, 24, 25, 26]. Because of the similarity of bioenergetic processes between bacteria and mitochondria, this effect can be associated with a decrease in the bacterial membrane potential as well as with the destabilization of the lipid membrane due to detergent-like effect or induction of non-specific permeability of the membrane at high concentrations of alkyl-TPP derivatives and an increase in alkyl chain length [18, 23, 24, 27].

Along with antibacterial properties, TPP derivatives of various structures have been reported to exhibit antiproliferative effects [28, 29, 30, 31]. Not only do the majority of cancer cells possess functional mitochondria, but the oncogenic transformation itself often increases mitochondrial metabolism [32]. The mitochondria of cancer cells may have increased transmembrane potentials in comparison with normal cells [33]. However, the bioenergetics of resistant and cancer stem cells (CSCs), which are mainly responsible for metastasis, are different from the cancer cells themselves [34, 35, 36]. Ultimately, this may allow cancer cells to be discriminated against according to the degree of aggressiveness. Conjugating TPP with various bioactive compounds [20, 30, 31] or nanocrystals [37] gives the chimeric molecules increased cellular accessibility and enhances their cytotoxicity against tumor cells. For that reason, TPP conjugates with paclitaxel [38] and doxorubicin [39] have recently been suggested to treat drug-resistant cancers. In turn, several TPP-containing compounds have been used to eliminate cancer stem cells (CSCs) [40]. A growing body of evidence has now shown that even at low concentrations, some antibiotics can cause mitochondrial dysfunction due to similarities in their structures with bacteria [41, 42]. On this basis, some mitochondria-targeting antibiotics have been used as anti-cancer drugs [43, 44]. Overall, the synthesis of compounds combining antibiotic derivatives with targeted delivery to mitochondria via TPP moiety could represent a novel approach in anti-cancer therapy, especially when applied to resistant forms of cancer.

CHL is a ribosome-targeting antibiotic that binds to the peptidyl transferase center (PTC) [45] of the bacterial ribosome and inhibits peptide bond formation [46]. CHL has been frequently used as a platform to obtain derivatives with increased potency [47]. This drug is especially amenable to chemical derivatization because its dichloracetyl moiety can be easily replaced with a variety of other chemical scaffolds, such as amino acids [48], peptides [49], or acyl group carrying a polyamine extension [50, 51], endowing it with new properties. Thus, the synthesis of novel CHL analogs containing triphenylphosphonium cation in their structure represents a promising challenge in terms of creating new potential dual-acting antibiotics and antiproliferative agents.

In the current study, we continued our research on the synthesis and exploration of semi-synthetic TPP analogs of CHL [1], CAM-Cn-TPPs, with the goal of obtaining a new group of CHL derivatives with potentially improved or even unique properties. To this end, the dichloromethyl group of the parent CHL compound was replaced with alkyl(triphenyl)phosphonium residues, resulting in CAM-Cn-TPP molecules (**Figure 1**). Using a competition binding assay, CAM-C10-TPP was shown to exhibit stronger binding to the bacterial ribosome compared to CHL, and the new CHL analogs also inhibited protein synthesis *in vitro*. Toeprinting assay revealed that the mode of action of CAM-Cn-TPP on the bacterial ribosome differs from the site-specific action of CHL, as previously shown for CAM-C4-TPP [1]. While the atomic-resolution structure of the ribosome-bound CAM-C4-TPP compound has been solved and reported recently, possible interactions of the other CAM-Cn-TPP compounds with the *E. coli* ribosome were modeled by molecular dynamics simulations. Using a potential-sensitive fluorescent probe,

 doi:10.20944/preprints202104.0026.v1

we found that CAM-C10-TPP and CAM-C14-TPP significantly reduce the membrane potential in *Bacillus subtilis* cells. Experiments with bacteria demonstrated that, in comparison to CHL, CAM-C10-TPP inhibited the growth of Gram-positive bacteria to a greater extent: *Staphylococcus aureus*, *Listeria monocytogenes*, *Bacillus subtilis,* and *Micobacteriym smegmatis*. In addition, CAM-C10-TPP and CAM-C14-TPP suppressed some strains of CHL-resistant bacteria. Thus, we showed that CAM-Cn-TPP compounds act both on the ribosome and on the cell membranes of bacteria, with the TPP fragments of CAM-C10-TPP and CAM-C14-TPP making a significant contribution to the inhibitory effect on bacterial growth. We also showed that TPP-derivatives could target mitochondria in chemoresistant breast cancer cells and derived cancer stem-like cells and reduce their proliferation.

Preprints (www.preprints.org) | NOT PEER-REVIEWED | Posted: 1 April 2021 doi:10.20944/preprints202104.0026.v1

2. Results and Discussion

2.1. Synthesis of CAM-Cn-TPPs

We have recently synthesized and extensively characterized the first semi-synthetic triphenylphosphonium (TPP) analogs of CHL, CAM-C4-TPP [1]. In the current study, we continued our research on the TPP analogs of CHL, synthesized two more of them, CAM-C10-TPP and CAM-C14-TPP, and explored their inhibitory properties for the potential development of novel antimicrobials as well as antiproliferative agents.

The dual-action mechanism of these compounds should be mediated, on the one hand, by their binding and action upon the bacterial ribosome (similar to the action of CHL), and, on the other hand, by their action on the bacterial membranes (similar to alkyl-TPP salts). To this end, the dichloromethyl group of CHL was replaced with alkyl-TPP moiety, resulting in CAM-Cn-TPP molecules (**Figure 1**).

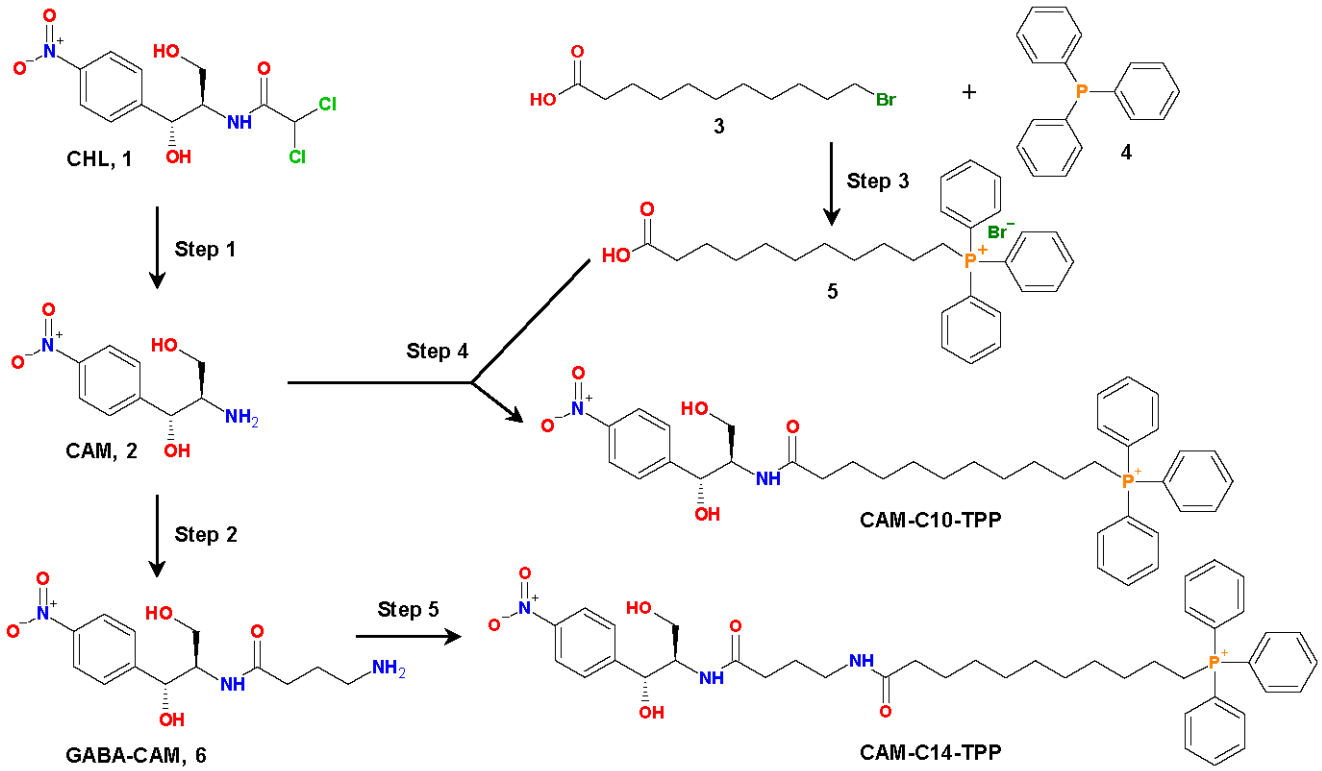

Figure 1. Scheme of chemical synthesis of triphenylphosphonium (TPP) analogues of CHL: CAM-C10-TPP and CAM-C14-TPP. Step 1: 1M hydrochloric acid (HCl) at 100°C for 2 hours. Step 2: 1) Boc-GABA-OSu, dimethylformamide (DMF), diisopropylethylamine (DIPEA) at 25°C for 24h, 2) trifluoroacetic acid (TFA) at 25°C for 30 minutes. Step 3: benzene at 85 °C for 72 h. Step 4: 1) 5, 1-hydroxysuccinimide (HOSu), N,N'-dicyclohexylcarbodiimide (DCC), dichloromethane (CH2Cl2) at 0°C for 2h, then overnight at RT 2) 2, DIPEA, DMF stirring at RT for 5h, then overnight at 4°C Step 5: 1) 5, HOSu, DCC, dichloromethane (CH2Cl2) at 0°C for 2h, then overnight at RT 2) 6, DIPEA, DMF stirring at RT for 5h, then stirring at 4°

These compounds were designed with the idea that the amphenicol moiety would anchor the compound in the canonical CHL binding site within the PTC of the bacterial ribosome, and an additional group would form multiple interactions with the walls of the nascent peptide exit tunnel (NPET). We've chosen TPP as such a group because of its positive charge delocalized over the relatively large hydrophobic surface of the benzene rings it could provide non-specific interactions with negatively charged phosphates of the 23S rRNA, and its three phenyl rings could be available for stacking with nucleobases. In the case of CAM-C4-TPP [1], we showed how this analog binds to the bacterial ri-

Preprints (www.preprints.org) | NOT PEER-REVIEWED | Posted: 1 April 2021 doi:10.20944/preprints202104.0026.v1

bosome and inhibits bacterial protein synthesis both *in vitro* and *in vivo.* Moreover, in accordance with our rational design hypothesis, the TPP group in these compounds should allow CAM-Cn-TPPs to enter bacterial cells since the TPP itself is known as a membrane penetrating cation [14].

As for the interactions with the ribosome, we expected that linkers of variable lengths connecting the two terminal parts of these compounds (CAM and TPP) would ensure optimal binding of CAM-Cn-TPPs to the ribosome and enable similar non-specific interactions with rRNA nucleotides at different NPET depths, as observed in the X-ray crystal structure of the *Thermus thermophilus* 70S ribosome in complex with the CAM-C4-TPP [1]. The choice of linker length was also based on the data on the inhibition of bacteria growth by alkyl-TPPs, where it was shown that the toxic effect on various bacterial species was upregulated with increasing lipophilicity, and this effect was related to different permeability of bacterial coats for alkyl-TPPs [18]. In addition, we modeled the length of the linkers using *in silico* simulations. Linkers with lengths of 10 (C10) and 14 (C14) methylene groups were chosen. In the latter case, an amide group was introduced to reduce possible side effects associated with the high lipophilicity of the resulting compound.

The synthesis of CAM-C10-TPP and CAM-C14-TPP was performed by acylation of chloramphenicol amine (CAM) with carboxyl derivatives of TPP using succinimide ester (Figure 1), similarly to the synthesis of CAM-C4-TPP [1]. The chemical structures of the obtained CAM-Cn-TPP molecules were confirmed by mass-spectrometric analysis as well as 1H-, 13C-, and 31P-NMR.

2.2. CAM-Cn-TPPs bind to the bacterial ribosome with different affinity and inhibit protein synthesis though allowing the formation of short peptides

All new semi-synthetic CAM-Cn-TPP compounds were expected to bind and act on the bacterial ribosomes inhibiting protein synthesis similar to CAM-C4-TPP and the PTC-targeting parent antibiotic CHL. To assess the affinity of CAM-C10-TPP and CAM-C14-TPP for the bacterial 70S ribosome (**Figure 2A**), we used a competition-binding assay exploiting BODIPY-labeled erythromycin (BODIPY-ERY) [52, 53, 48]. CAM-C10-TPP was found to have significantly higher (~7-fold) affinity to the ribosome compared to parent CHL and slightly higher (~1.5-fold) compared to CAM-C4-TPP (K_{Dapp} = 0.4 ± 0.04 μM for CAM-C10-TPP vs. 2.8 ± 0.4 μM for CHL and K_{Dapp} = 0.61 ± 0.07 μM for CAM-C4-TPP [1]). Unexpectedly, CAM-C14-TPP binds to 70S ribosome with significantly lower affinity compared to other CAM-Cn-TPPs (~60-90-fold) and CHL (~13-fold, K_{Dapp} = 36 ± 9 μM for CAM-C14-TPP). It is likely that in the case of CAM-C14-TPP, the linker might be too long, preventing the optimal positioning of the TPP moiety in the NPET. Thus, CAM-C10-TPP and CAM-C14-TPP both bind to the bacterial ribosome. However, their affinity strongly depends on the length of the linker connecting the two chromophores. Among the three CAM-Cn-TPPs, the C10-linker was optimal for the ability of the compound to bind to the 70S ribosome.

Next, we tested the effects of CAM-C10-TPP and CAM-C14-TPP in bacterial cells by using the *E. coli ΔtolC*-based reporter system, which is designed to screen inhibitors targeting either protein synthesis or DNA replication [54]. In this reporter system, a gene of the far-red fluorescent protein, *katushka2S*, is inserted downstream of the genetically modified tryptophan attenuator that makes possible expression of Katushka2S only upon exposure to ribosome-stalling compounds (**Figure 2B**, CHL and ERY, red pseudocolor rings); the red fluorescent protein gene *rfp* is placed under the control of the SOS-inducible sulA promoter that allows detecting expression of Red Fluorescent Protein (RFP) reporter under the action of corresponding compounds, such as inhibitors of DNA gyrase (e.g., levofloxacin, LEV, **Figure 2B**, green pseudocolor ring).

We used chloramphenicol amine (CAM), N-acetyl-chloramphenicol amine (CAM-Ac), and alkyl-TPP (C10-TPP and C14-TPP) as negative controls in this assay. We observed neither induction of any of the two reporters (no colored rings) nor inhibition of

Preprints (www.preprints.org) | NOT PEER-REVIEWED | Posted: 1 April 2021 doi:10.20944/preprints202104.0026.v1

cell growth by CAM or CAM-Ac (no dark zone in the middle). This indicates that the removal of the two Cl atoms from the dichloroacetyl group of CHL makes it inactive [55]. The C10-TPP and C14-TPP compounds (lacking the CAM moiety) inhibit bacterial cell growth (dark area in the middle) but do not induce either of the two reporters, suggesting that they act through an entirely different cellular target (likely target the membrane [18]). For CAM-C10-TPP and CAM-C14-TPP, as well as for the positive controls CHL and ERY, red pseudocolor rings are observed due to expression of the fluorescent protein Katushka2S (but not RFP), indicating that these compounds specifically inhibit protein synthesis as was previously observed for CAM-C4-TPP [1].

The next step was to test the new CAM-Cn-TPP compounds for their ability to inhibit the synthesis of the firefly luciferase reporter i*n vitro* in a cell-free transcription-translation system based on *E. coli* S30 extract. CAM-C10-TPP, as well as CAM-14-TPP, inhibited bacterial translation similar to CHL (**Figures 2C**) and CAM-C4-TPP [1]. At the same time, both CAM-C10-TPP and CAM-C14-TPP compounds exhibited no effect on eukaryotic *in vitro* translation (**Figure 2C**), which was revealed by a similar approach using eukaryotic *in vitro* translation system.

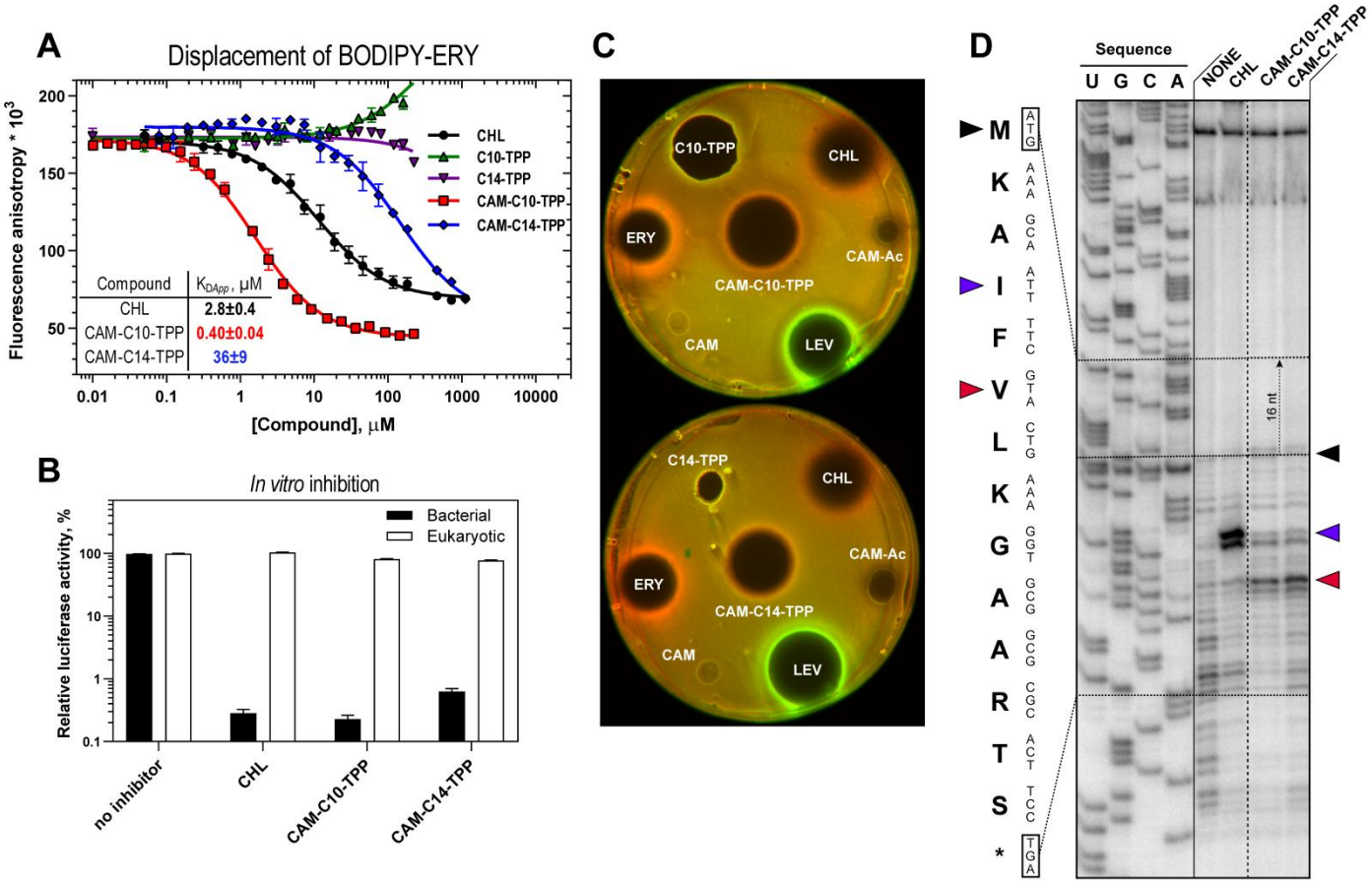

Figure 2. Binding affinity to bacterial ribosomes and inhibition of protein synthesis by CAM-C10-TPP and CAM-C14-TPP. (**A)** Competition-binding assay to test the displacement of fluorescently labeled analogs of erythromicyn, BODIPY-ERY, from the *E. coli* 70S ribosomes in the presence of increasing concentrations of CHL (black circles), CAM-C10-TPP (red squares), CAM-C14-TPP (blue rhombus), decyl(triphenyl)phosphonium bromide (C10TPP, green triangles) or tetradecyl(triphenyl)phosphonium bromide (C14TPP, purple triangles) measured by fluorescence anisotropy. All reactions were repeated four times. Error bars represent standard deviation. The resulting values for apparent dissociation constants (K_{Dapp}) are shown on each plot. (**B**) Testing of CAM-C10-TPP and CAM-C14-TPP activity using *E. coli BW25113 ΔtolC pDualRep2* reporter strains. The induction of the red fluorescent protein expression (green halo around the inhibition zone, pseudocolor) is triggered by DNA-damage while the induction of Katushka2S protein (red halo) occurs in response to ribosome stalling. Levofloxacin (LEV), erythromycin (ERY), chloramphenicol (CHL),

Preprints (www.preprints.org) | NOT PEER-REVIEWED | Posted: 1 April 2021 doi:10.20944/preprints202104.0026.v1

N-acetyl-chloramphenicol amine (CAM-Ac), C10TPP and C14TPP are used as controls. (**C**) Inhibition of protein synthesis by 30 μM of CHL, CAM-C10-TPP or CAM-C14-TPP *in vitro* in the cell-free bacterial (black columns) and eukaryotic (transparent columns) transcription-translation coupled system. The relative enzymatic activity of *in vitro* synthesized firefly luciferase is shown. Error-bars represent standard deviations of the mean of three independent measurements. (**D**) Ribosome stalling by CAM-Cn-TPP on *trpL* mRNA in comparison with CHL, revealed by reverse-transcription primer-extension inhibition (toeprinting) assay in a cell-free translation system. Nucleotide sequences of *trpL* mRNA and its corresponding amino acid sequence is shown on the left. Black arrowhead marks translation arrest at the start codon, while colored arrowheads point to the drug-induced arrest sites within the coding sequences of mRNAs used. Note that due to the large size of the ribosome, the reverse transcriptase used in the toeprinting assay stops 16 nucleotides downstream of the codon located in the P-site.

Recently it was shown that the mechanism of action of CHL on translation is different from what was previously widely accepted (blocking accommodation of the incoming aminoacyl-tRNA in the PTC): in the presence of CHL, short peptides can be synthesized on the ribosome, and the action of the antibiotic is context-specific [56]. CHL arrests translation only when alanine, and to a lesser extent, serine or threonine appear in the penultimate position (E site) of the growing polypeptide chain and only if there is no glycyl-tRNA in the A site of the ribosome [56]. As shown in our recent study, the action of CAM-C4-TPP on bacterial translation was also context-specific, but its mode of action is different from the site-specific action of CHL [1].

To investigate the mechanism of action of CAM-C10-TPP and CAM-C14-TPP on the translation process, primer extension inhibition assay (toeprinting) was used. This method allows unambiguous identification of the drug-induced ribosome stalling sites along the mRNA with a single nucleotide precision [57]. This technique is also used to determine the context-specificity of antibiotic action [56]. For this experiment, we chose *trpL* mRNAs as the template, as in the pDualrep2 reporter system. Unlike CHL, which stalls ribosomes at the Ile5 codon (**Figures 2D** and **S1**, blue arrowhead) of the corresponding Ala4 in the penultimate position of the growing polypeptide chains (E-site), CAM-10-TPP, CAM-14-TPP, and CAM-C4-TPP, blocked ribosome progression at Val7 and slightly at Ile5 (**Figure 2D**, red arrowhead. Compared to the results previously obtained for CAM-C4-TPP using *rst1* and *rst2* mRNA templates [1], more unambiguous results were obtained using *trpL* mRNA template. The main drug-induced ribosome stalling sites are different for CHL and CAM-Cn-TPP, and there are also CAM-Cn-TPP-specific stalling positions. These results support the conclusion that CAM-Cn-TPPs have an idiosyncratic mode of action and their unique context-specificity that differs from that of the original CHL [1].

2.3. Possible dynamics of CAM-Cn-TPPs interaction during translation

To assess the possible interactions of CAM-Cn-TPPs with the ribosome during translation, we modeled the structures of complexes of the new compounds, CAM-C10-TPP and CAM-C14-TPP, with the *E. coli* 70S ribosome by molecular dynamics simulations. To this end, we used a structure of *E. coli* 70S ribosome in the classical non-rotated a/A-p/P-state, which is conformationally similar to the ribosome containing tRNAs during translation [58]. Analysis of the most populated clusters (**Figure 3**, **Table S1**) for the CAM-Cn-TPP complexes revealed that all these compounds are able to interact quite stably with the non-canonical CHL binding site [59]. The CAM-C10-TPP complex is characterized by the most stable stacking interactions and hydrogen bonding and is similar to the analogous CHL complex. Obviously, the positive charge of the TPP fragment is responsible for the nonspecific affinity of all CAM-Cn-TPPs to the negatively charged rRNA.

CAM-Cn-TPPs were constructed as bidentate ligands differing in the length of the flexible alkyl chain linking CAM- and TPP- moieties. The synergism of interactions of these two basic structural elements with one or another region of the NPET depends on the length of the CAM-Cn-TPP linker. Thus, the relatively long and flexible alkyl chain of CAM-C10-TPP allows the CAM and TPP residues to adapt to their binding sites in the NPET (**Figures 3A,B**). On the contrary, the longer linker in the CAM-C14-TPP structure

Preprints (www.preprints.org) | NOT PEER-REVIEWED | Posted: 1 April 2021 doi:10.20944/preprints202104.0026.v1

results in the inability of this compound to fit snugly in the space between the optimally bound CAM and TPP fragments. These findings may explain the higher affinity of the CAM-C10-TPP to the bacterial ribosomes compared to the CAM-C14-TPP.

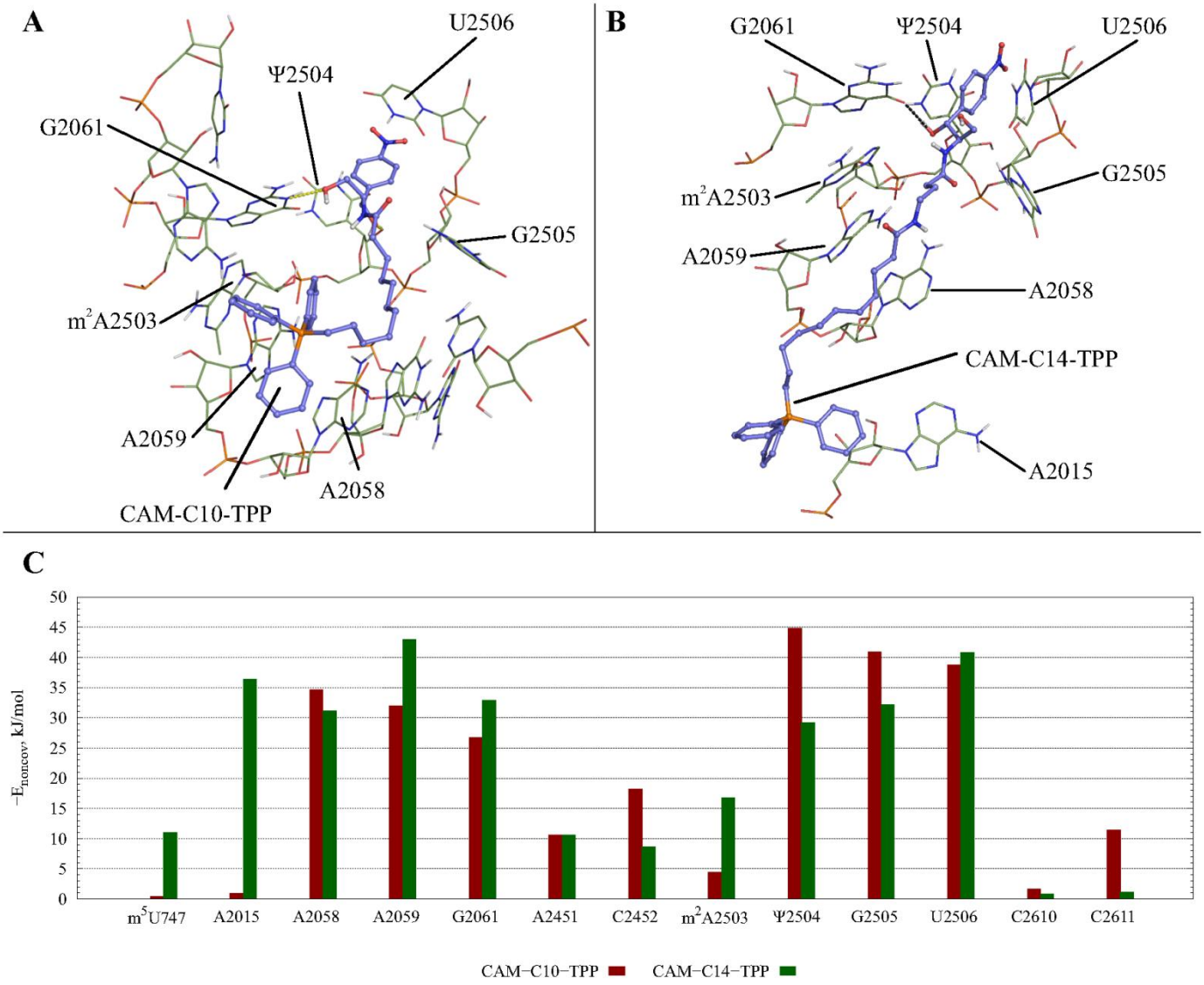

Figure 3. Interactions between CAM-C10-TPP (A), CAM-C14-TPP (B) and *E. coli* A,A/P,P–ribosome, obtained by MD simulations. Hydrogen bonds are shown by black dashes. CAM-Cn-TPP nitrophenyl fragment is immersed in the "hydrophobic cavity" formed by Ψ2504 and U2506 bases, forming stacking interactions with them. The arrangement of hydrogen bonds for the CAM-C10-TPP complex (**A**) corresponds to the non-canonically linked CHL [59]. For CAM-C14-TPP a stable hydrogen bond between O1-hydroxyl group of CAM residue and O6 of G2061 is observed. The TPP fragment of CAM-C10-TPP interact with the "hydrophobic cavity" of the macrolide binding site, forming developed hydrophobic contacts with A2058, A2059 and C2610 bases. The long C14-linker in CAM-14-TPP appears in the "hydrophobic cavity" between A2058 and A2059 bases, and the TPP fragment is located deeper in the NPET adjacent to the residue A2015. (**C**) Energy of noncovalent interactions between CAM-C10-TPP (red columns) or CAM-C14-TPP (green columns) and neighboring 23S rRNA residues of *E. coli* ribosome that are in the canonical A,A/P,P– state. E_{noncov} is shown with a negative sign for improved readability.

It is noteworthy that models of CAM-Cn-TPPs complexes with *E. coli* ribosome staying in the canonical A,A/P,P–state described above are in agreement with foregoing data on translation arrest in the presence of CAM-C10-TPP and CAM-C14-TPP (**Figure 2D**), and of CAM-C4-TPP described in [1]. For all three mRNA templates, *trpL* for CAM-C10-TPP and CAM-C14-TPP, and *trpL*,*rst1* and *rst2* for CAM-C4-TPP, the peptides synthesized before arrest contain sequences corresponding to -2 to -5 codon regions (2 to

Preprints (www.preprints.org) | NOT PEER-REVIEWED | Posted: 1 April 2021 doi:10.20944/preprints202104.0026.v1

5 amino acid residues from the C-terminus of nascent peptide), consisting of amino acids mainly with hydrophobic and aromatic side groups, which may be near CAM-Cn-TPP during translation in NPET. These positions are occupied by the A−4IF−2 in the case of *trp*L, W−5VT−3 in the case of *rst1* and F−5AI−3 in the case of *rst2* templates. Obviously, these amino acids are capable of forming hydrophobic contacts with the TPP residue of CAM-Cn-TPP, so that nascent peptide can bind firmly in the NPET, hindering translation.

2.4. CAM-CnTPP cause a decrease in the membrane potential of B. subtilis

As noted in the Introduction, alkyl-TPPs and their derivatives exhibit an antibacterial effect, which is associated with a decrease in the membrane potential of bacteria [18, 23, 24]. Thus, we further examined the effect of CAM-Cn-TPP on bacterial membrane potential of *B. subtilis*. In particular, the membrane potential of *B. subtilis* can be estimated from the fluorescence of the potential-sensitive dye DiS-C3-(5) by measurement the changing fluorescence. The potential-dependent accumulation of the dye inside the bacterial cell causes quenching and leads to a decrease in fluorescence. Under the influence of substances that reduce the membrane potential, the dye is released and the fluorescence increases. As shown in **Figure 4**, submicromolar concentrations of CAM-C10-TPP and CAM-C14-TPP caused a decrease in the membrane potential of *B. subtilis* on a minute time scale, whereas 10 μM CAM-C10-TPP or CAM-C14-TPP caused a rapid drop of membrane potential to the level observed with the channel-forming antibiotic gramicidin A, which is known to vanish the bacterial membrane potential while CAM-C4-TPP begins to act only at high (10μM or more) concentrations. Therefore, the action of CAM-Cn-TPP can have a double effect on bacterial cells and be based on the depolarization of the bacterial membrane by analogy with the mechanism of action of Cn-TPP [18].

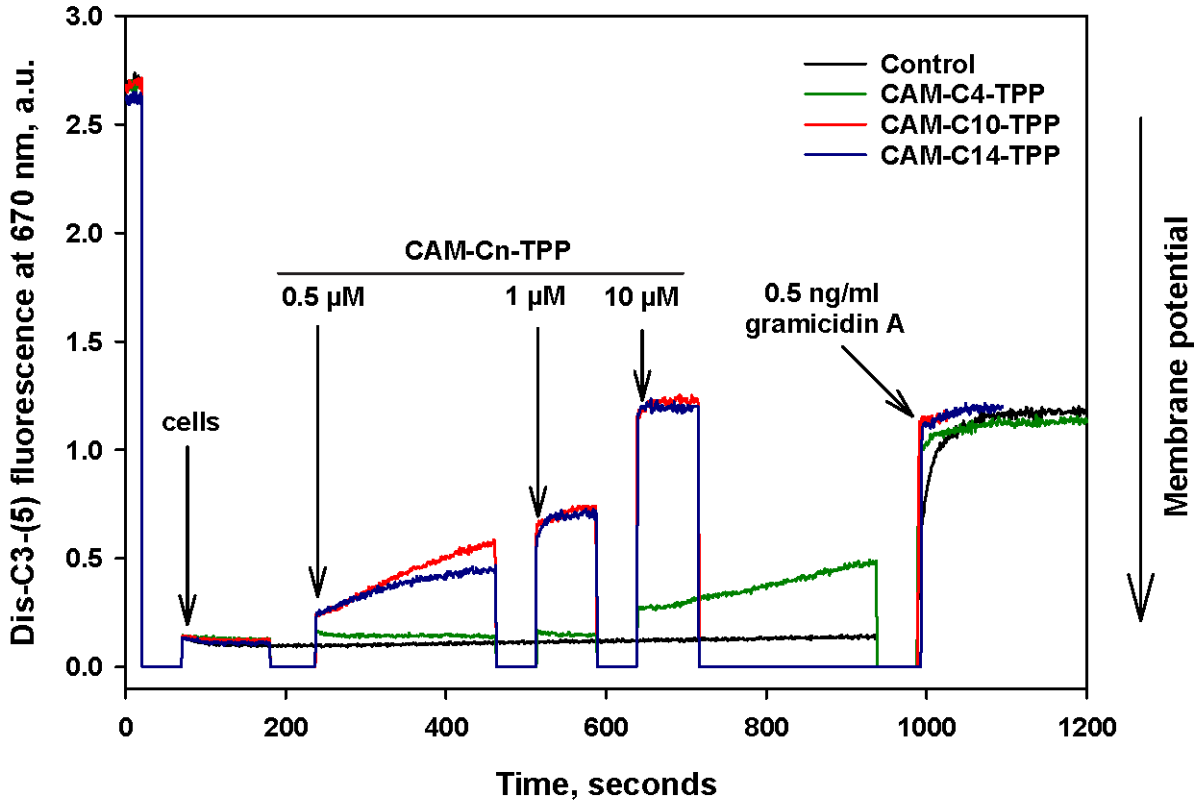

Figure 4. Dose-dependent effect of CAM-Cn-TPP on the kinetics of the membrane potential of *B. subtilis* cells assessed by DiS-C3-(5) (10 μM) fluorescence in PBS buffer. To reach desired concentrations, appropriate amounts of CAM-Cn-TPP were added at the moment marked by arrows. Gramicidin A concentration was 50 ng/ml.

2.5. CAM-C10-TPP and CAM-C14-TPP inhibit bacterial growth

Preprints (www.preprints.org) | NOT PEER-REVIEWED | Posted: 1 April 2021 doi:10.20944/preprints202104.0026.v1

In order to check whether the synthesized compounds are antimicrobial agents, we tested their action on a number of bacterial species (**Tables 1**, **2** and **S2**). Both CHL and alkyl-TPPs are known to act on Gram-positive bacteria [50, 18] CAM-C10-TPP and CAM-C14-TPP were found to be able to inhibit the growth of *S.aureus*, *L.monocytogenes*, *B.subtilis* and *Mycobacterium sp.* strains. Moreover, CAM-C10-TPP suppressed bacterial growth more effectively than CHL, depending on the strain (**Table 1**). It was also found that CAM-C10-TPP inhibit CHL-resistant *E.coli* strains (**Table S2**).

Table 1. Suppression of the growth of Gram-positive bacteria by CAM-Cn-TPPs. Values of minimal inhibitory concentration (MIC, μM) are shown[1].

	Staphylococcus aureus	*Listeria monocytogenes*	*Bacillus subtilis*	*Mycobacterium smegmatis*
CHL	60	25	12	6
CAM-C10-TPP	5	6	2	2
CAM-C14-TPP	12	17	12	8
C10-TPP	2	5	2	<2
C14-TPP	1,6	2	8	4

[1] MIC values were determined using the double-dilution method. The MIC for each compound was determined in triplicate in two independent sets.

These findings prompted us to further investigate the antibacterial activity of CAM-Cn-TPP on CHL-resistant strains of *B. subtilis* and *E. coli* strains with deletions of TolC genes and, therefore, more sensitive to the action of compounds that can otherwise be pumped out from the Gram-negative bacterial cells by a dedicated efflux pump TolC. AcrAB-TolC is the main multi-drug resistance transporter of Gram-negative bacteria, which is responsible for the efflux of C10-TPP derivatives [19, 60]. Apparently, the efflux of CAM-Cn-TPP is also mediated by this transporter, but the degree of involvement of other TolC-containing transporters in CAM-Cn-TPP efflux has not yet been clearly defined.

Table 2. Suppression of the growth of *E.coli* strains with the deletion of *tolC* gene and harboring CHL acetyltransferase (*cat*) gene (*E.coli ΔtolC-CAT*), or *B.subtilis* CHL resistant strains (*B.subtilis pHT01-cat*) and harboring methyltransferase Cfr *(cfr)* gene (*B.subtilis pHT01-cfr*) by CAM-Cn-TPPs. Values of minimal inhibitory concentration (MIC, μM) are shown[1].

	E.coli ΔtolC	*E.coli ΔtolC-CAT*	*Bacillus subtilis*	*B.subtilis pHT01-cat*	*B.subtilis pHT01-cfr*
CHL	2,8	>360	12	180	90
CAM-C10-TPP	3	25	2	6	6
CAM-C14-TPP	12,5	12,5	12	12,5	6
C10-TPP	3	3	2	1,6	0,8
C14-TPP	1,6	6	8	1,6	0,8

[1] MIC values were determined using the double-dilution method. The MIC for each compound was determined in triplicate in two independent sets

E. coli ΔtolC CHL-resistant strain harboring plasmid encoding for chloramphenicol acetyltransferase (*cat*) *(pCA24N-LacZ)* and control *E. coli ΔtolC* strain was used to evaluate the inhibitory effect of compounds. CHL-resistant strains of *B. subtilis pHT01-cat* and *B. subtilis pHT01-cfr* were prepared by means of transformation of a *B. subtilis 168* strain with plasmids harboring *cat* and *cfr* genes (chloramphenicol-florfenicol resistance) gene. The *cfr* gene encodes for the methyltransferase that catalyzes methylation of m^2A2503 in the 23S rRNA and causes resistance to a variety of ribosome-targeting antibiotics that bind in the A site of the bacterial ribosome [61].

As follows from the data shown in **Table 2**, CAM-C10-TPP inhibited growth of the *E. coli ΔtolC* strain with the same efficiency as CHL, and CAM-C14-TPP with a slightly

Preprints (www.preprints.org) | NOT PEER-REVIEWED | Posted: 1 April 2021 doi:10.20944/preprints202104.0026.v1

lower. In contrast, CAM-Cn-TPPs were significantly more effective against CHL-resistant strains in comparison with CHL. At the same time, MIC values for Cn-TPP on all tested strains were lower than those of CAM-Cn-TPPs. A similar effect was observed for CHL-resistant *B. subtilis* because of the presence of *cat* or *cfr* genes. While CAM-Cn-TPPs clearly inhibit protein biosynthesis in bacteria *in vitro*, damage to bacterial membranes due to the presence of an alkyl-TPP fragment in their structure contributes more to the action of CAM-Cn-TPPs at the cellular level.

If we compare the TPP analogs of CHL with the nearest structural analogs exhibiting antimicrobial activity, in the structure of which two pharmacophores are conjugated via the alkyl linker, we can note that an antibacterial effect of these compounds is due to the fact that they either bind to bacterial ribosomes or inhibit translation in bacteria, as do polyamide analogs of CHL [50, 51], or disrupt the bacterial membrane potential, as alkyl TPP conjugates with fluorescein [23, 24] or coumarin [21, 22], while CAM-Cn-TPPs have the ability to exhibit both of these effects.

2.6. CAM-10-TPP and CAM-14-TPP show reduced toxicity compared to alkylTPP on mammalian cells in MTT-assay

As we have already shown, CAM-Cn-TPPs have no noticeable effect on the eukaryotic translation process (**Figure 2C**). Given the obvious antibacterial activity of CAM-C10-TPP and CAM-C14-TPP, it was important to assess their cytotoxicity for mammalian cells. The Mosman ("MTT") assay was used for this purpose [62].

CAM-C10-TPP and CAM-C14-TPP are more toxic to various eukaryotic cell lines in comparison to CHL (**Table 3**) but at the same time significantly less toxic than the well-known cytotoxic drug doxorubicin, which we used as a high toxicity control. Notably, CAM-Cn-TPPs were less toxic than the corresponding alkyl-TPPs, which are part of molecular structures of these analogs and were also used (as bromides) as control compounds. Alkyl-TPPs are known to be quite toxic, and the toxicity effect seems to be mainly due to their ability to accumulate in the mitochondria [63, 64]. On the other hand, this effect may be caused by a decrease of cellular metabolism under the influence of TPP derivatives which may be a consequence of the charge change on the cell membrane, i.e. the same effect that provides them antibacterial properties [25, 26, 27]. Thus, it cannot be ruled out that CAM-Cn-TPP also can disrupt cell adhesion due to a decrease in the charge on the membrane due to positively charged phosphonium cations. The lower toxicity of the synthesized analogs against mammalian cells, compared to alkyl-TPPs, is a favorable property in terms of considering CAM-Cn-TPPs as antimicrobial compounds.

Table 3. Growth inhibition by CAM-Cn-TPPs in relation to a number of cell lines according to the MTT assay. Values of 50% growth inhibition concentration (GI50, μM) are shown.

	HEK293T	***MCF7***	***A549***	***VA13***
CHL	>50	>50	>50	>50
CAM-C10-TPP	0,62 ± 0,04	0,97 ± 0,14	0,65 ± 0,1	2,75 ± 0,48
CAM-C14-TPP	3,59 ± 0,46	5,84 ± 0,84	2,92 ± 0,38	5,2 ± 0,88
C10-TPP	0,08 ± 0.01	0,21 ± 0,03	0,07 ± 0.01	0,27 ± 0,05
C14-TPP	0,03 ± 0.02	0,02 ± 0,01	0,025 ± 0.009	0,067 ± 0,05
Doxorubicin	0,007 ± 0,001	0,044 ± 0,012	0,041 ± 0,010	0,176 ± 0,042

On the other hand, the relatively high toxicity of CAM-Cn-TPP to human adenocarcinoma cells (MCF7 and A549, **Table 3**) may indicate that these compounds can be used as antiproliferative agents. CAM-C10-TPP and CAM-C14-TPP has about 4-2 times selectivity of action between cancerous A549 and noncancerous VA13 cell lines. These results correspond to previous reports [65, 66] that DLCs may have selective cytotoxicity against cancer cells. Otherwise, there was no selectivity of their action on the cancerous cell lines

 doi:10.20944/preprints202104.0026.v1

in comparison with HEK293T cells of noncancerous etiology but compatible to cancerous cells growth rate.

2.7. Anticancer activities of CAM-C10-TPP and CAM-C14-TPP

We recently provided *in vivo* [67] and *in vitro* [68] evidence that some bactericidal antibiotics suppress tumor growth by causing mitochondrial dysfunction. Our results showed that antibiotics preferentially suppress the growth of cancer chemoresistant and the so-called cancer stem cells (CSC), the two main categories of cells responsible for cancer recurrence and metastasis [42]. These cells differ from their respective parental cells and display a different response to the same microenvironmental stimuli allowing them to reduce their proliferating rate and survive chemotherapeutic treatment. Here, we tested the above TPP-CAM derivatives on chemoresistant triple negative breast cancer (TNBC) cell models, as well as on corresponding CSC-like spheroid cells. We have created several corresponding models based on TNBC cell lines, in particular MDA-MB-231 and BT-549, in their resistance to cyclophosphamide. To create CSC-like cells, parental cells were resuspended in nonadherent conditions to form tumorspheres. We applied the TPP derivatives and found that both CAM-C10-TPP and CAM-C14-TPP, but not CAM-C4-TPP significantly reduced proliferation of TNBC cell lines (**Figure 5**). We also noticed that higher concentrations of derivatives preferentially inhibited proliferation of chemoresistant rather than parental cancer cells.

Preprints (www.preprints.org) | NOT PEER-REVIEWED | Posted: 1 April 2021 doi:10.20944/preprints202104.0026.v1

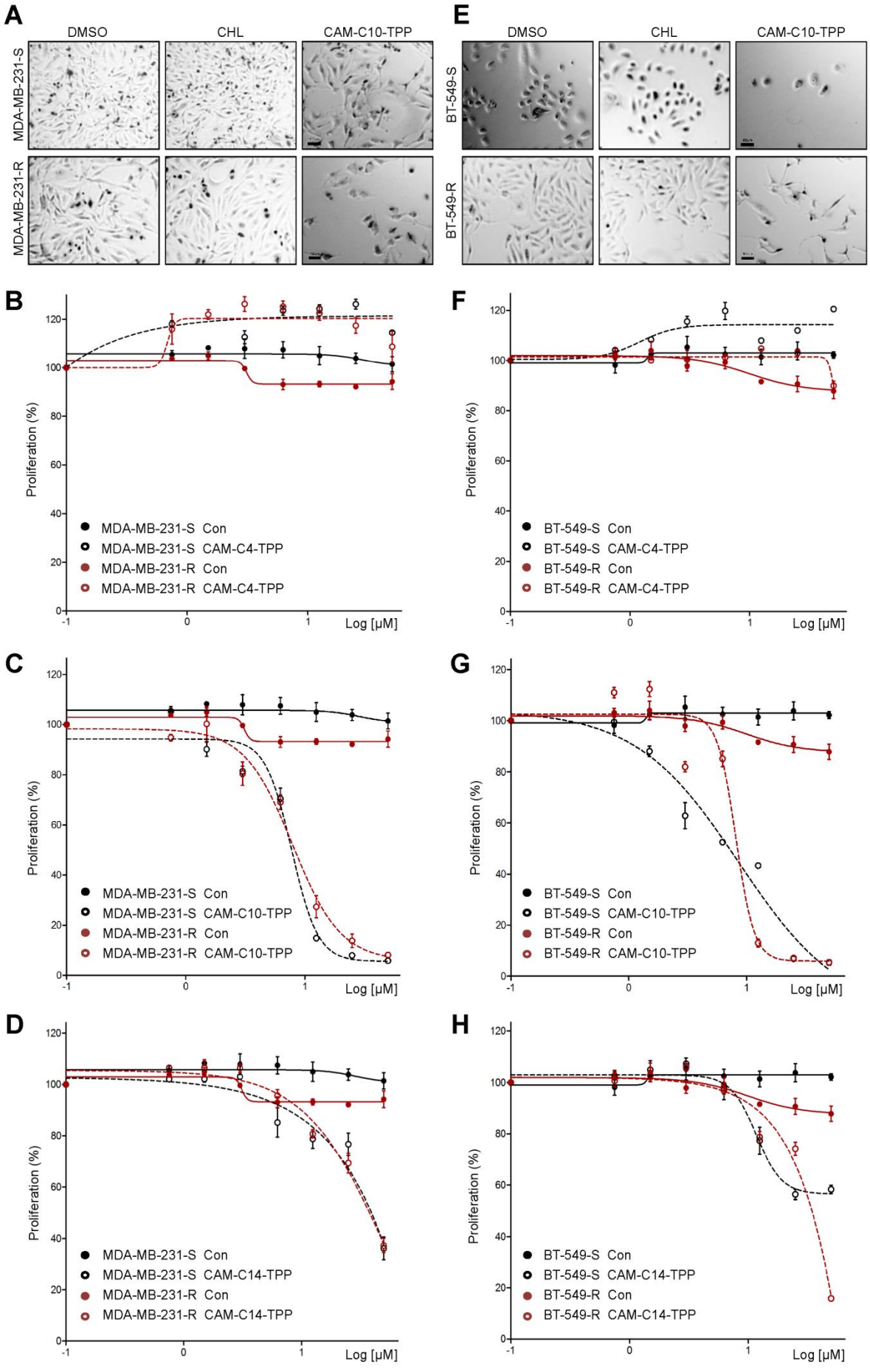

 doi:10.20944/preprints202104.0026.v1

Figure 5. Effect of CAM-TPP derivatives on cell viability in TNBC cells. MDA-MB-231 (A-D) and BT-549 (E-H) TNBC sensitive (S) and chemoresistant (R) cells were grown at 60% confluence for 3 days with the indicated concentrations of CAM-TPP derivatives. Representative images (A, E) were obtained at 40× magnification. The scale bar 10um. Cells were subjected to viability assays. Results represent the mean of 3 independent experiments. Data indicate the mean ± SEM. P-values, all relative to controls, were statistically significant ($P < 0.05$).

Several TPP-containing compounds have been proposed for the elimination of CSCs by the Lisanti group [40]. In the current work, we studied the effect of CAM-TPP derivatives on CSC-like TNBC cell models. We found a significant decrease in spheroid formation when exposed to CAM-C10-TPP (also to CAM-C14-TPP) (**Figure 6A**, **E**). The same compounds reduced the survival of CSCs formed from parental and resistant TNBC cell lines (**Figure 6B-D**, **F-H**).

Preprints (www.preprints.org) | NOT PEER-REVIEWED | Posted: 1 April 2021 doi:10.20944/preprints202104.0026.v1

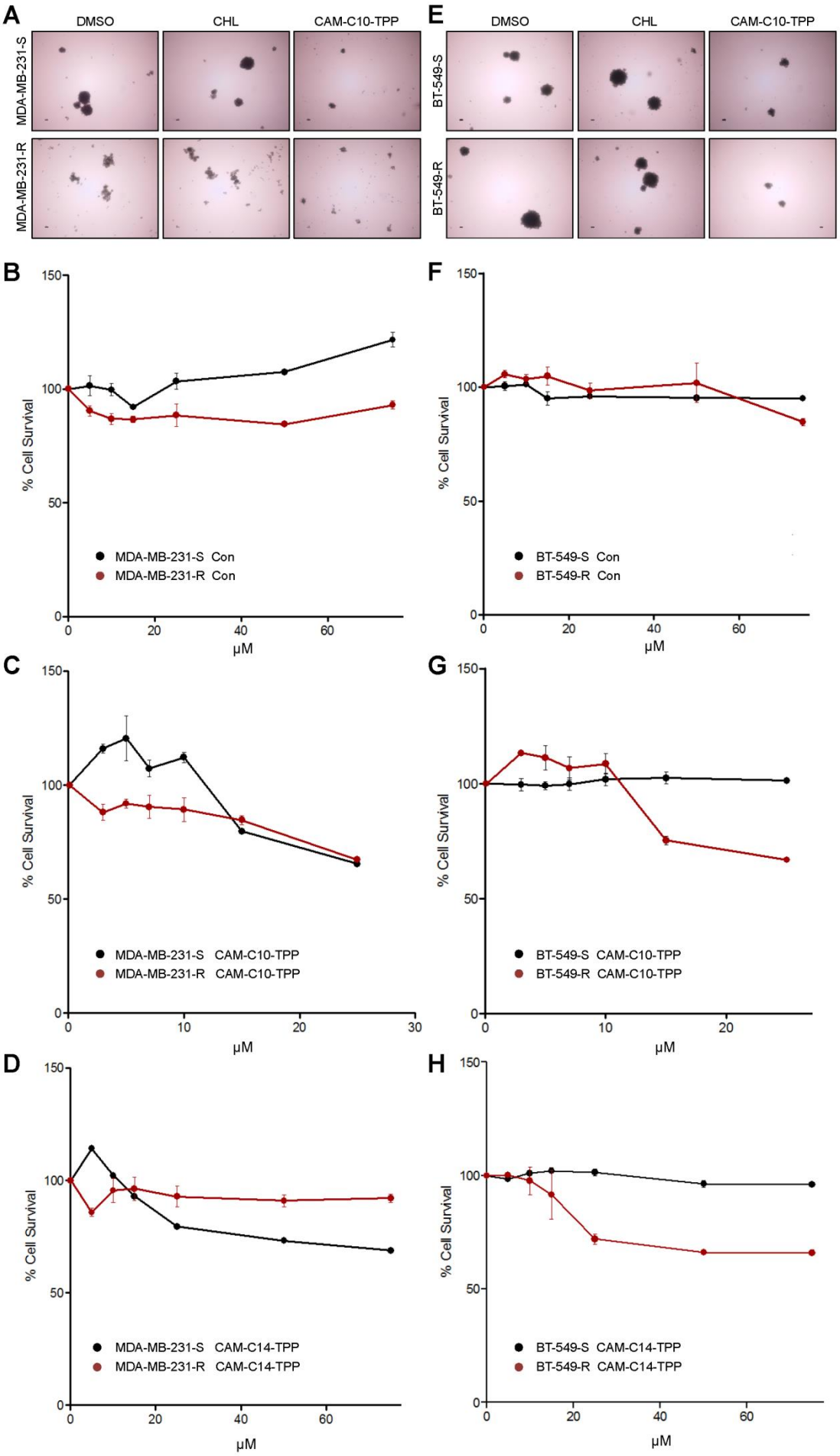

Preprints (www.preprints.org) | NOT PEER-REVIEWED | Posted: 1 April 2021 doi:10.20944/preprints202104.0026.v1

Figure 6. Effect of CAM-TPP derivatives on cell viability in CSC-like TNBC cells. MDA-MB-231 (A-D) and BT-549 (E-H) TNBC sensitive (S) and chemoresistant (R) cells were grown under non-adherent conditions for 5 days in the presence of CAM-TPP derivatives to form spheroids. Representative images (A, E) of CAM-C10-TPP-treated cells show a decrease in spheroid size. CSC-like cells were then tested for viability as before. Results are the mean of 3 independent experiments Data indicate the mean ± SEM. P-values, all relative to controls, were statistically significant ($P < 0.05$).

It should be noted that antiproliferative activity was also detected in TPP and Cn-TPP itself, which seems to be related to depolarization of the mitochondrial membrane potential [28, 29, 30, 31]. In this regard, we consider these data on the use of CAM-Cn-TPP derivatives as one of the possible approaches to anti-cancer therapy requiring more careful study and titration of concentrations and doses. Overall, our data suggest that specific targeting of cancer cell mitochondria with dual-acting compounds may have clinical advantages for drug development against resistant forms of cancer.

3. Materials and Methods

3.1. Chemicals and materials

The following reagents were used: chloramphenicol (Sigma); 1-hydroxysuccinimide (HOSu), N,N'-dicyclohexylcarbodiimide (DCC) and 4-aminobutyric acid (GABA) (Fluka), triphenylphosphine and 11-bromundecanoic acid (Acros Organics). The fluorescent erythromycin derivative BODIPY-Ery was obtained previously [69]. Alkyl-TPPs were obtained according to [18].

3.2. Synthetic procedures

The scheme for the synthesis of chloramphenicol triphenyphosphonium analogues (CAM-C10-TPP, CAM-C14-TPP) is represented in **Figure 1**. (1R,2R)-2-amino-1-(4-nitrophenyl)propane-1,3-diol (chloramphenicol amine, CAM, 2) was obtained *via* the acid hydrolysis of chloramphenicol (CHL, 1) according a procedure [55] as described in [53, 48]. (10-carboxydecyl)(triphenyl)phosphanium bromide (**5**) was obtained by condensation of 11-bromoundecanoic acid (**3)** and triphenylphosphin (**4**) during 12 h at 85°C.

(N-{[(1R,2R)-1,3-dihydroxy-1-(4-nitrophenyl)propan-2-yl]amino}-11-oxoundecyl)(triphenyl)phosphonium bromide (CAM-C10-TPP). To the cold solution of 140 mg (0,25 mmol) of (10-carboxydecyl)(triphenyl)phosphanium bromide (**5**) and 30 mg (0,25 mmol) of HOSu in 5 ml of anhydrous CH_2Cl_2 62 mg (0,3 mmol) of DCC was added at 0°C. The mixture was stirred for 2 h at 0°C and overnight at RT. The formed precipitate was filtered off, and the solvent was removed *in vacuo*. The residue was dissolved in 1 ml of DMF, then 62,5 mg (0,25 mmol) of CAM (**2**) and 52,8 μl (0,375 mmol) DIPEA in 250 μl of DMF was added and the resulted mixture was stirred for 5h at RT and overnight at 4°C. Then the reaction mixture was diluted with 15 ml of water and 1N aqueous HCl was added dropwise to neutral pH. Then the mixture was extracted with $CHCl_3$ (3×15 ml), and the combined organic extracts were washed with water (3×10 ml). Organic layer was dried over anhydrous Na_2SO_4, the volatiles were evaporated in vacuo. The target product was isolated from residue by purification on silica gel column eluting with solvents system $CHCl_3$: MeOH, 6:1.Yield: 123 mg (73%); TLC: R_f ($CHCl_3$: MeOH, 6:1) 0.3, R_f (CH_3Cl : MeOH, 9:1) 0.26; LC-MS m/z calculated for $C_{32}H_{34}N_2O_5P$ $(M)^+$ 641.3, found 641.4; t_R = 1.08 min; ESI-MS m/z calculated for $C_{38}H_{46}O_5NP$ $(M)^+$: 641.3133, found 641,3149.

N-[(1R,2R)-1,3-dihydroxy-1-(4-nitrophenyl)propan-2-yl]-4-(triphenyl)phosphoniumundecanamidobutamide bromide (CAM-C14-TPP) was obtained as CAM-10-TPP from 263 mg (0,5 mmol) (10-carboxydecyl)(triphenyl)phosphanium bromide (**5**), 58 mg (0,5 mmol) of HOSu, 103 mg (0,5 mmol) of DCC, 200 mg (0,5 mmol) of GABA-CAM·TFA (**6**) and 253 μl (1,42 mmol)of DIPEA. The target product was isolated on silica gel column eluting with solvents system CHCl3 : MeOH : NH4OH = 65:25:4 Yield: 261 мг (65%); TLC: R_f ($CHCl_3$: MeOH, 5:1) 0.53 , R_f(CHCl3 : MeOH : NH_4OH, 65:25:4) 0.7; LC-MS m/z calculated for

Preprints (www.preprints.org) | NOT PEER-REVIEWED | Posted: 1 April 2021 doi:10.20944/preprints202104.0026.v1

$C_{42}H_{53}N_3O_6P$ $(M)^+$ 726,4 , found 726,7; t_R = 0,50 min ; ESI-MS m/z calculated for $C_{42}H_{53}N_3O_6P$ $(M)^+$: 726,3667, found 726,3692.

See also Supplementary Materials for more detailed procedures, characteristics, and NMR-data.

3.3. In vitro binding assay

Binding affinity of CAM-Cn-TPP to *E. coli* ribosomes was analyzed by competition binding assay using fluorescently-labeled BODIPY-ERY as described before [52, 69, 53, 48]. BODIPY-Ery (16 nM) or BODIPY-CAM (30 nM) was incubated with the ribosomes (50 nM or 2.9 μM respectively) in the buffer for 30 min at 25 °C. Solutions of CHL, CAM-Cn-TPP and CnTPP in different concentration ranges were added to the formed complex. The mixture was incubated for 2 h until equilibrium was reached and the values of fluorescence anisotropy were measured. Dissociation constants were calculated based on the assumption of equilibrium competitive binding of two ligands at a single binding site as described in [70].

3.4. Detection of the translation inhibitors with pDualrep2 reporter

Reporter strain *JW55035* [71] *ΔtolC (BW25113) pDualrep2* was used as previously described [72]. Tested antibiotics CAM-C10-TPP (10 mM, 1.5 μl), CAM-C14-TPP (10 mM, 1.5 μl), C10-TPP (10 mM, 1.5 μl), C14-TPP (10 mM, 1.5 μl), CAM (10 mM, 1.5 μl), CAM-Ac (10 mM, 1.5 μl), chloramphenicol (CHL, 2 mM, 1 μl) erythromycin (Ery, 7 mM, 1 μl), levofloxacin (Lev, 70 nM, 1 μl) were applied to an agar plate that already contained a lawn of the reporter strain. After being incubated overnight at 37 °C, the plate was scanned by ChemiDoc (Bio-Rad) in the modes "Cy3-blot" for RFP and "Cy5-blot" for Katushka2S.

3.5. In vitro translation inhibition assay and toeprinting assays

Inhibition of firefly luciferase synthesis in cell-free translation systems by CAM-Cn-TPP was tested with *E. coli* S30 Extract System for Linear Templates (Promega). Reactions were programmed with 100 ng mRNA and were carried out in 5 μL aliquots at 37 °C for 30 minutes. The activity of *in vitro* synthesized luciferase was assessed using 5 μL of the substrate from the Steady-Glo Luciferase Assay System (Promega).

Inhibition of eukaryotic translation was measured in Rabbit Reticulocyte Lysate (Promega) according to the manufacturer's protocol. Reactions were programmed with 100 ng Fluc mRNA and were carried out in 5 μL aliquots at 37 °C for 30 minutes. The activity of *in vitro* synthesized luciferase was assessed using 5 μL of the substrate from the Steady-Glo Luciferase Assay System (Promega).

The toeprinting assay was carried out using *trpL* mRNA as a template as described in [73], reactions were preincubated for 5 min with 30 μM of the tested compound.

3.6. Bacteria inhibition assays

3.6.1. Bacterial strains.

To prepare bacterial suspension, bacteria stock cultures were sub-cultured onto plates with proper agar medium and incubated overnight at 30 °C or 37 °C until reaching optical density 1.5 (at 600 nm), which was measured on Varioskan LUX microplate reader (Thermo Scientific, USA) or an Ultrospec 1100 pro spectrophotometer (Amersham Biosciences Corp., USA).

Standard laboratory strains *Bacillus subtilis* subs. *subtilis* Cohn 1872, stains *BR151*, and *168*, *Staphylococcus aureus* subsp. *aureus* Rosenbach 1884 strains *JCM 2151* and entry MC#144 (from the Microorganisms Collection of the Moscow State University), *Listeria monocytogenes* Pirie 1940, *Mycobacterium smegmatis* Lehmann & Neumann 1899 (MC#377) and *Escherichia coli* Castellani and Chalmers 1919, strain *JW5503* (with the deletion of tolC gene), and resistant to chloramphenicol strains *J53rif*, *C600rif/pIB55-1*, *C600rif/pIP162-1*, *C600recA naI* were used.

Preprints (www.preprints.org) | NOT PEER-REVIEWED | Posted: 1 April 2021 doi:10.20944/preprints202104.0026.v1

S. aureus was grown in Bacto Tryptic Soy Broth, *L. monocytogenes* in Brain Heart Infusion Broth and *E. coli* in LB. Bacterial cells were grown at 30 °C or 37 °C in the appropriate medium at 140 rpm shaking frequency.

Standard laboratory strain *E.coli JW5503* with the deletion of *tolC* gene, referred here as *ΔtolC* strain, was used to get *ΔtolC pCA24N-LacZ* strain by means of transformation with the plasmid pCA24N-LacZ harboring chloramphenicol acetyltransferase (*cat*) gene.

Standard laboratory strain *B.subtilis 168* was used to obtain CHL resistant strains *B.subtilis pHT01-CAT* and *B.subtilis pHT01-cfr* by means of transformation with the corresponding plasmids. Competent cell preparation and transformation procedures were conducted as reported in [74, 75]. Desired colonies were selected at 10 μg/ml CHL for *B.subtilis pHT01* and 5 μg/ml or 3.2 μg/ml CHL for *B.subtilis pHT01-cfr*.

3.6.2. Plasmids

pcan24N-lacZ was purified from *JW0335* strain (ASKA- collection), *pHT01* (was kindly provided by Dr. Svetlana Dubiley), pHT01-cfr plasmid was obtained by the following procedure. The whole pHT01 plasmid sequence was amplified with primers 5′-TTGATATGCCTCCTAAATTTTTATC-3' and 5'-TATGAGATAATGCCGACTG-3′. Cfr gene was amplified with primers 5′- acagtcggcattatctcataCTATTGGCTATTTTGATAATTACC-3′ and 5′-aaatttaggaggcatatcaaATGAATTTTAATAATAAAACAAAGTATGG-3′ using *Staphylococcus sp. (cfr+)* genome DNA as a template. Joining of two DNA fragments was performed with NEBuilder HiFi DNA Assembly Master Mix (NEB) and subsequent selection of right clones.

3.6.3. CAM-Cn-TPP-dependent bacterial growth suppression screening of TolC-requiring transporters.

E. coli deletion mutants' panel [19, 60] was selected. Selected bacterial strains belonging to the panel were diluted in fresh LB media after overnight growing. 200 μl of bacterial cell cultures (5 * 105 cells/ml) were inoculated into 96-well plates. Preselected CAM-C14-TPP and CAM-C10-TPP concentrations (5 μM, 10μM, and 20 μM) were added to each mutant and optical density at 620 nm was measured using a Thermo Scientific Multiskan FC plate reader. Cells were left to grow for 21 hours at 37 °C and optical density at 620 nm was measured. All experiments were performed at least in triplicates.

3.6.4. MIC determination.

MICs for CAM-Cn-TPP and Cn-TPP were determined by Mueller-Hinton broth microdilution, as recommended by CLSI in Methods for Dilution Antimicrobial Susceptibility Tests for Bacteria that Grow Aerobically, Approved Standard, 9th ed., CLSI document M07-A9, using in-house-prepared panels. The compounds were diluted in a 96-well microtiter plate to final concentrations ranging from 0.5 to 360 μM in 250-μl aliquot of the bacterial suspension followed by the incubation at 37 °C or 30 °C for 18 h. MIC was determined as the lowest concentration that completely inhibited bacterial growth. Bacterial growth was observed visually alongside with OD measurements. Experiments were carried out in triplicate.

3.7. Measurement of B. subtilis membrane potential

Membrane potential in *B. subtilis* was estimated by measuring fluorescence of the potential-dependent probe DiS-C3-(5) [76]. *B. subtilis* from the overnight culture were seeded into fresh LB medium, followed by growth for 24 h until reaching the optical density 0.8 at 600 nm. Then the bacteria were diluted 20-fold in a buffer containing 100 mM KCl, 10 mM Tris, pH 7.4. Fluorescence was measured at 670 nm (excitation at 630 nm) by using a Fluorat-02-Panorama fluorimeter.

3.8. In vitro survival assay (MTT assay)

The cytotoxicity of tested substances was tested using the MTT (3-(4,5-dimethylthiazol-2-yl)2,5-diphenyl tetrazolium bromide) assay [62] with some modifications. 2500 cells per well for MCF7, HEK293T and A549 cell lines, or 4000 cells

Preprints (www.preprints.org) | NOT PEER-REVIEWED | Posted: 1 April 2021 doi:10.20944/preprints202104.0026.v1

per well for VA-13 cell line were plated out in 135 µl of DMEM-F12 media (Gibco, USA) in 96-well plate and incubated in the 5% CO_2 incubator for first 16 h without treating. Then 15 µl of media-DMSO solutions of tested substances to the cells (final DMSO concentrations in the media were 1% or less) and treated cells 72 h with 25 nM - 50 µM (eight dilutions) of our substances (triplicate each), serial DMSO dilutions and doxorubicin were used like controls. The MTT reagent (Paneco LLC, Russia) then was added to cells up to final concentration of 0.5 g/l (10X stock solution in PBS was used) and incubated for 2.5 h at 37 °C in the incubator, under an atmosphere of 5% CO_2. The MTT solution was then discarded and 140 µl of DMSO (PharmaMed LLC, Russia) was added. The plates were swayed on a shaker (60 rpm) to dissolve the formazan. The absorbance was measured using a microplate reader (VICTOR X5 Light Plate Reader, PerkinElmer, USA) at a wavelength of 565 nm (in order to measure formazan concentration). The results were used to construct a dose-response graph and to estimate CC_{50} value.

3.9. Cancer cell proliferation assays

3.9.1. Cell lines and tumoursphere formation

MDA-MB-231 (RRID: CVCL_0062) and BT-549 (RRID: CVCL_1092) cell lines were purchased from ATCC and cultured in DMEM/F12 (Gibco, Life Technologies, 31330-038) supplemented with 10% FBS, 1% Pen-Strep, 1% Sodium Pyruvate and 1% L-glutamine. Chemoresistant cell lines were established with continuous treatment for 6 months with anticancer therapeutic agents, cyclophosphamide (Rcyclo), as previously described [67]. These cell lines were authenticated using short tandem repeat (STR) profiling within the last three years. To obtain CSC-like cells, a single cell suspension was prepared using enzymatic disaggregation (1x Trypsin-EDTA, Gibco, 25300062) and cells were plated at a density of 10.000-12.000 cells per ml in Cancer Stem Cell medium (C-28070, PromoCell, Heidelberg, Germany) in poly-2-hydroxyethyl methacrylate (Poly-HEMA, Santa Cruz Biotechnology, sc-253284) coated plates. Cells of the first generation (G1) were collected 10 days after seeding. Cells were transfected with corresponding compounds or DMSO (control) followed by the above procedure of tumoursphere formation. Relative numbers of tumourspheres per well were counted manually. Experiments were performed independently for at least 2 times with several replicates.

3.9.2. Cancer cell proliferation

Survival assay was performed essentially as described earlier [77]. In short, cells were seeded into a 96-well plate followed by treatment with increased concentrations of corresponding CAM-TPP derivatives for 3 days. 3-(4,5-dimethyltiazolyl-2)-2,5-diphenyltetrazolium bromide (0.5 mg/ml MTT; Sigma-Aldrich) dissolved in media was added to each well. Following incubation for 2 h, the supernatant was carefully removed from the wells, and 100 µl of DMSO:ethanol mix (1:1) was added to each well followed by shaking for 10 min. Absorbance was measured at 570 nm in Bio Spec 1601, Shimadzu spectrometer. The OD570 of the DMSO solution in each well was considered to be proportional to the number of cells. The OD570 of the control (treatment without supplement) was considered 100%. The results were expressed as means ± SD. Data was analyzed with GraphPad Prism 7 PRIZM computer software under the license of Statistical Department (Vall' d Hebron Hospital).

3.10. Molecular dynamics simulations

The structure of *E. coli* AP–ribosome modeled in [78] was used. A cubic fragment was extracted from this structure in the same manner as in the cited work. CAM-Cn-TPPs, **Figure S2** (atom numbering is based on [79]) were docked into this ribosome fragment using rDock [80] package with 1000 runs of the optimization process. Then pose of sequent CAM-Cn-TPP, which show the highest predicted affinity to the ribosome among other poses of same compound, was placed in the above described fragment of ribosome. The constructed system was centered in a tetragonal cell with dimension of 9.1×9.1×10 nm, so, when it was filled with water, edgges of the ribosome

Preprints (www.preprints.org) | NOT PEER-REVIEWED | Posted: 1 April 2021 doi:10.20944/preprints202104.0026.v1

fragment were covered by at least 0.9 nm thick solvent layer. During molecular dynamics simulations residues having at least one atom located within 0.1 nm from the edge of the simulated ribosome fragment were positionally restrained. Such approach preserves the local conformatonal movability of rRNA residues which is adequate to fit their conformations to binding ligand.

Equilibrium molecular dynamics simulation of 200 ns length was performed for every constructed system, coordinates of simulated system were recorded every 25 ps with integration time step of 2 fs. Lengths of covalent bonds with hydrogen atoms were limited by the LINCS algorithm [81]. Velocity rescaling thermostat with additional stochastic term [82] at constant temperature of 300 K and 0.1 ps coupling time was applied during simulation, the Berendsen barostat [83] with 5 ps coupling time was used to support isotropic constant pressure with periodic boundary conditions. The particle mesh Ewald algorith with 0.125 nm grid step and the fourth order interpolation was used to threat long–range electrostatic interactions [84]. TIP4P*EW* water was used as a solvent. Potassium ions with optimized parameters [85] were added to neutralize residual negative charge of system, and they were placed near negatively charged groups [86]. To prevent elution of magnesium and potassium counterions into the aqueous phase, part of the water molecules were randomly replaced with magnesium, potassium and chlorine ions, setting the concentrations of $MgCl_2$ at 7 mM and KCl at 100 mM.

Canonical and modified amino acid and nucleotide residues were modeled with parm99sb [87], while CAM-Cn-TPPs was modeled with the GAFF force field [88]. Optimized three dimensional structures and molecular electrostatic potentials of the newly parameterized residues and compounds were prepared by quantum chemical Hartree-Fock calculations with the 6–31G* basis set. Partial charges were evaluated with the RESP model [89].

GROMACS [90, 91] software version 5.1.4 was used to simulate molecular dynamics simulations and analysis of obtained trajectories, including analysis of hydrogen bonds and stacking interactions performed in the same way as in [92], clustering of frames by GROMOS [93] method and calculation of energy of noncovalent interactions: $E_{noncov} = E_{VdW} + E_{Coulomb}$.

4. Conclusions

Based on our recent findings on the study of CAM-C4-TPP [1], in this work, we set out to create dual-acting antimicrobial compounds, the structure of which would include an amphenicol fragment of CHL and a triphenylphosphonium cation, connected by linkers of different lengths, CAM-Cn-TPP. We synthesized CAM-C10-TPP and CAM-C14-TPP, and examined their ribosome binding and translation inhibitory properties, as well as their action on the bacterial membrane. CAM-C10-TPP and CAM-C14-TPP bind to the bacterial ribosome, and their affinity depends on the length of the linker connecting the two chromophores. The new CHL analogs inhibit protein synthesis *in vitro* like CAM-C4-TPP, allowing the formation of few peptide bonds, but the mode of action of CAM-Cn-TPP on bacterial ribosome differs from the site-specific action of CHL as has been observed earlier for CAM-C4-TPP. Moreover, we showed that CAM-C10-TPP inhibited the growth of the Gram-positive bacteria: *Staphylococcus aureus*, *Listeria monocytogenes*, *Bacillus subtilis* and *Micobacteriym smegmatis*, stronger than CHL, and both CAM-C10-TPP and CAM-C14-TPP inhibited some strains of CHL-resistant bacteria. Withal, we found that CAM-C10-TPP and CAM-C14-TPP caused a significant drop of the membrane potential in *Bacillus subtilis* cells, and, apparently, this effect makes the main contribution to the antibacterial action of the new compounds. Thus, we showed that on the basis of a ribosome antibiotic (CHL) and a penetrating cation (triphenylphosphonium), antimicrobial agents acting simultaneously on the bacterial ribosome and on the bacterial membrane could be obtained. This approach could be developed in the future to create new antibacterial agents by reducing the toxicity of compounds, for example, us-

ing other more physiological penetrating cations, as well as, possibly, new antiproliferative agents.

Supplementary Materials: The following are available online at www.mdpi.com/xxx/s1: Detailed procedures of the synthesis and NMR-data; **Table S1**: Occurrences of hydrogen bonds and stacking interactions of CAM-Cn-TPP, obtained by MD simulations; **Table S2**: Suppression of the growth of CHLresistant *E.coli* strains harboring CHL acetyltransferase (*cat*) gene by CAM-C10-TPP (MIC, μM); **Figure S1**: Original version of the Figure 2D; **Figure S2**: Triphenylphosphonium derivatives of chloramphenicol amine: CAM–C10-TPP (A), CAM–C14–TPP (B).

Author Contributions: synthesis, N.V.S., J.A.P.; purification, N.V.S., J.A.P.; binding assay, A.G.T., J.A.P.; translation inhibition assay, I.A.O., J.A.P.; toeprinting analysis, D.A.L., I.A.O, J.A.P.; membrane potential assays, J.A.P., P.A.N.; 70S ribosomes preparation, A.L.K., A.P.; MTT-tests, D.A.S.; bacteria inhibition assays, Z.Z.K., J.A.P.,P.A.N., I.A.V., I.A.O.; cancer cell proliferation assays, A.L., E.A.; molecular dynamics modelling, G.I.M.;. supervision, N.V.S., I.A.O., A.A.B.; writing—original draft preparation, N.V.S., A.G.T., I.A.O., G.I.M, P.A.N, A.L..; writing—review and editing, N.V.S., I.A.O., P.A.N., D.A.S., A.L., Y.N.A., A.A.B. All authors have read and agreed to the published version of the manuscript.

Funding: This research was funded by RFBR [grants 20-04-00873 to N.V.S. (synthesis of analogs, binding assays, *in vitro* translation), 20-015-00537 to P.A.N. (potential measurement, screening of TolC-containing transporters) and 20-54-76002 to I.A.O. (toeprinting and *in vitro* translation)], President grant MD 2626.2021.1.4 to I.A.O. (bacteria inhibition assays), grants from the Instituto de Salud Carlos III: PI17/02087 to A.L. (cancer cell proliferation assays), by the Ministry of Science and Higher Education of the Russian Federation [grant FENU-2020-0019 to G.I.M. (molecular dynamics simulations)] and by the Government of the Russian Federation [No. AAAA-A17-117120570004-6 to A.A.B.].

Acknowledgments: We thank Dr. Yury Polikanov for the critical reading of the manuscript and valuable feedback. We thank V.N. Tashlitsky for LCMS analyses, Yu.K. Grishin and V.I. Polshakov for NMR spectra, Medved'ko A.V. and M.A. Sukonnikov for polarimetric data, I.V. Plyushchenko and I.A. Rodin for high-resolution MS, A. Zalevsky for software arranging cations on nucleic acids, and the Research Computing Center at Lomonosov Moscow State University for the opportunity to perform molecular dynamics simulations using the "Lomonosov–II" supercomputer. This study was carried out using equipment purchased with funds from Lomonosov Moscow State University Development Program.

Conflicts of Interest: The authors declare no conflict of interest.

References

1. Chen, C.-W.; Pavlova, J.A.; Lukianov, D.A.; Tereshchenkov, A.G.; Makarov, G.I.; Khairullina, Z.Z.; Tashlitsky, V.N.; Paleskava, A.; Konevega A.L.; Bogdanov, A.A.; Osterman, I.A.; Sumbatyan, N.V.; Polikanov, Y.S. Binding and action of triphenylphosphonium analog of chloramphenicol upon the bacterial ribosome suggest new ways for rational drug design. *Antibiotics* **2021**, 10 (accepted for publication).
2. Gabibov, A.G.; Dontsova, O.A.; Egorov, A.M. Overcoming antibiotic resistance in microorganisms: molecular mechanisms. *Biochemistry (Moscow)* **2020**, *85*, 1289-1291. DOI: 10.1134/S0006297920110012
3. Wilson, D.N. Ribosome-targeting antibiotics and mechanisms of bacterial resistance. *Nat. Rev. Microbiol.* **2013**, *12*, 35–48. DOI: 10.1038/nrmicro3155
4. Lewis, K. At the Crossroads of Bioenergetics and Antibiotic Discovery. *Biochemistry (Moscow, Russ. Fed.)* **2020**, 85, 1469–1483. DOI: 10.1134/S0006297920120019
5. Barbachyn, M.R. Recent advances in the discovery of hybrid antibacterial agents. In *Annual Reports in Medicinal Chemistry*, Macor J. E.; Eds.; Elsevier Academic Press: San Diego, USA, 2008; 281–290. DOI: 10.1016/S0065-7743(08)00017-1
6. Pokrovskaya, V.; Baasov, T. Dual-acting hybrid antibiotics: a promising strategy to combat bacterial resistance. *Expert Opinion on Drug Discovery* **2010**, 5, 883–902. DOI: 10.1517/17460441.2010.508069
7. Tevyashova, A.N.; Olsufyeva, E.N.; Preobrazhenskaya, M.N. Design of dual action antibiotics as an approach to search for new promising drugs. *Russ. Chem. Rev.* **2015**, 84, 61–97. DOI: 10.1070/RCR4448
8. Parkes, A.L.; Yule, I.A. Hybrid antibiotics – clinical progress and novel designs. *Expert Opinion on Drug Discovery* **2016**, 11, 665–80. DOI: 10.1080/17460441.2016.1187597
9. Tevyashova, A.N.; Bychkova, E.N.; Korolev, A.M.; Isakova, E.B.; Mirchink P.E.; Osterman I.A.; Erdei, R.; Szücs, Z.; Batta, G. Synthesis and evaluation of biological activity for dual-acting antibiotics on the basis of azithromycin and glycopeptides. *Bioorg. Med. Chem. Lett.* **2019**, 29, 276–280. DOI: 10.1016/j.bmcl.2018.11.038

10. Bremner, J.B.; Ambrus, J.I.; Samosorn, S. Dual action-based approaches to antibacterial agents. *Curr. Med. Chem.* **2007**, 14, 1459-1477. DOI: 10.2174/092986707780831168
11. Lewis, K. Persister Cells. *Annu. Rev. Microbiol.* **2010**, 64, 357–372. DOI: 10.1146/annurev.micro.112408.134306
12. Datta, P.; Gupta, V. Next-generation strategy for treating drug resistant bacteria: Antibiotic hybrids. *Indian Journal of Medical Research* **2019**, 149, 97-106. DOI: 10.4103/ijmr.IJMR_755_18
13. Efimova, S. S.; Tevyashova, A. N.; Olsufyeva, E. N.; Bykov E. E.; Ostroumova O. S. Pore-forming activity of new conjugate antibiotics based on amphotericin B. *PLoS One* **2017**, 12, e0188573. DOI: 10.1371/journal.pone.0188573
14. Liberman, E. A.; Topaly, V. P.; Tsofina, L. M.; Jasaitis, A. A.; Skulachev, V. P. Mechanism of Coupling of Oxidative Phosphorylation and the Membrane Potential of Mitochondria. *Nature* **1969**, 222, 1076–1078. DOI: 10.1038/2221076a0
15. Feniouk, B.A.; Skulachev, V.P. Cellular and Molecular Mechanisms of Action of Mitochondria-Targeted Antioxidants. *Current Aging Science* **2017**, 10, 41–48. DOI: 10.2174/1874609809666160921113706
16. Murphy, M.P.; Smith, R.A.J. Targeting Antioxidants to Mitochondria by Conjugation to Lipophilic Cations. *Annu Rev Pharmacol Toxicol* **2007**, 47, 629–656. DOI: 10.1146/annurev.pharmtox.47.120505.105110
17. Severin, F.F.; Severina, I.I.; Antonenko, Y.N.; Rokitskaya, T.I.; Cherepanov, D.A.; Mokhova, E.N.; Vyssokikh, M.Y.; Pustovidko, A.V.; Markova, O.V.; Yaguzhinsky, L.S.; Korshunova, G.A.; Sumbatyan, N.V.; Skulachev, M.V.; Skulachev V.P. Penetrating cation/fatty acid anion pair as a mitochondria-targeted protonophore. *Proceedings of the National Academy of Sciences* **2009**, 107, 663–668. DOI: 10.1073/pnas.0910216107
18. Khailova, L.S.; Nazarov, P.A.; Sumbatyan, N.V.; Korshunova, G.A.; Rokitskaya, T.I.; Dedukhova, V.I.; Antonenko, Y.N.; Skulachev, V.P. Uncoupling and toxic action of alkyltriphenylphosphonium cations on mitochondria and the bacterium *Bacillus subtilis* as a function of alkyl chain length. *Biochemistry (Moscow, Russ. Fed.)* **2015**, 80, 1589–1597. DOI: 10.1134/S000629791512007X
19. Nazarov, P.A.; Osterman, I.A.; Tokarchuk, A.V.; Karakozova, M.V.; Korshunova, G.A.; Lyamzaev, K.G.; Skulachev, M.V.; Kotova, E.A.; Skulachev, V.P.; Antonenko, Y.N. Mitochondria-targeted antioxidants as highly effective antibiotics. *Sci Rep* **2017**, 7, 1394. DOI: 10.1038/s41598-017-00802-8
20. Kolesińska, B.; Motylski, R.; Kamiński, Z.J.; Kwinkowski, M.; Kaca, W. Synthesis of P-triazinylphosphonium salts-hybrid molecules with potential antimicrobial activity. *Acta Pol Pharm.* **2011**, 68, 387-391. https://pubmed.ncbi.nlm.nih.gov/21648193/.
21. Kumari, S.; Jayakumar, S.; Gupta, G.D.; Bihani, S.C.; Sharma, D.; Kutala, V.K.; Sandur, S.K.; Kumar, V. Antibacterial activity of new structural class of semisynthetic molecule, triphenyl-phosphonium conjugated diarylheptanoid. *Free Radical Biol. Med.* **2019**, 1, 140-145. DOI: 10.1016/j.freeradbiomed.2019.08.003
22. Kumari, S.; Jayakumar, S.; Bihani, S.C.; Shetake, N.; Naidu, R.; Kutala, V.K.; Sarma, H.D.; Gupta, G.D.; Sandur, S.K.; Kumar, V. Pharmacological characterization of a structurally new class of antibacterial compound, triphenyl-phosphonium conjugated diarylheptanoid: Antibacterial activity and molecular mechanism. *J Biosci.* **2020**, 45, 147. PMID: 33410424. DOI: 10.1007/s12038-020-00113-7
23. Nazarov, P.A.; Kirsanov, R.S.; Denisov, S.S.; Khailova, L.S.; Karakozova, M.V.; Lyamzaev, K.G.; Korshunova, G.A.; Lukyanov, K.A.; Kotova, E.A.; Antonenko, Y.N. Fluorescein derivatives as antibacterial agents acting via membrane depolarization. *Biomolecules* **2020**, 10, 309. doi: 10.3390/biom10020309
24. Iaubasarova, I.R.; Khailova, L.S.; Nazarov, P.A.; Rokitskaya, T.I.; Silachev, D.N.; Danilina, T.I.; Plotnikov, E.Y.; Denisov, S.S.; Kirsanov, R.S.; Korshunova, G.A.; Kotova, E.A.; Zorov, D.B.; Antonenko, Y. N. Linking 7-nitrobenzo-2-oxa-1,3-diazole (NBD) to triphenylphosphonium yields mitochondria-targeted protonophore and antibacterial agent. *Biochemistry (Moscow, Russ. Fed.)* **2020**, 85, 1578–1590. DOI: 10.1134/S000629792012010X
25. Churilov, M.N.; Denisenko, Y.V.; Batyushin, M.M.; Bren, A.B.; Chistyakov, V.A. Prospects of SkQ1 (10- (6′-plastoquinoyl) decyltriphenylphosphonium) application for prevention of oral cavity diseases. *Rasayan J. Chem.* **2018**, 11, 1594–1603. DOI: 10.31788/RJC.2018.1144077
26. Kang, S.; Sunwoo, K.; Jung, Y.; Hur, J.K.; Park, K.H.; Kim, J.S.; Kim, D. Membrane-targeting triphenylphosphonium functionalized ciprofloxacin for methicillin-resistant *Staphylococcus aure*us (MRSA). *Antibiotics (Basel)* **2020**, 9, 758. DOI: 10.3390/antibiotics9110758
27. Pinto, T.; Banerjee, A.; Nazarov, P.A. Triphenyl phosphonium-based substances are alternatives to common antibiotics. *Bull. Russ. State Med. Univ.* **2018**, 7, 16–25. DOI: 10.24075/brsmu.2018.003
28. Balczewski, P.; Skalik, J.; Nawrot, B.; Cieslak, M.; Kazmierczak-Baranska, J. Triphenylphosphonium salts for use in cancer therapy. European patent office 15460043.1, Aug 2015.
29. Sparey, T.; Ratcliffe, A.; Hallett, D.; Cochrane, E.; Lassalle, G.; Frodbise, A.; Stevenson, B. Triphenylphosphonium-tethered tetracyclines for use in treating cancer. World Intellectual Property Organization PCT/EP20 18/06023 1, Oct 2018.
30. Tsepaeva, O.V.; Nemtarev, A.V.; Salikhova, T.I.; Abdullin, T.I.; Grigor Eva, L.R.; Khozyainova, S.A.; Mironov, V.F. Synthesis, Anticancer, and antibacterial activity of betulinic and betulonic acid c-28-triphenylphosphonium conjugates with variable alkyl linker length. *Anticancer Agents Med Chem.* **2020**, 20, 286-300. DOI: 10.2174/1871520619666191014153554
31. Tsepaeva, O.V.; Salikhova, T.I.; Grigor'eva, L.R.; Ponomaryov, D.V.; Dang, T.; Ishkaeva, R.A.; Abdullin, T.I.; Nemtarev, A.V.; Mironov, V.F. Synthesis and *in vitro* evaluation of triphenylphosphonium derivatives of acetylsalicylic and salicylic acids: structure-dependent interactions with cancer cells, bacteria, and mitochondria. *Med Chem Res* **2021**, 30, 925–939. DOI: 10.1007/s00044-020-02674-6

32. Weinberg, S.E.; Chandel, N.S. Targeting mitochondria metabolism for cancer therapy. *Nat. Chem. Biol* **2015**, 11, 9-15. DOI: 10.1038/nchembio.1712
33. Dairkee, S.H.; Hackett, A.J. Differential retention of rhodamine 123 by breast carcinoma and normal human mammary tissue. *Breast Cancer Res. Treat.* **1991**, 18, 57-61. DOI: 10.1007/BF01975444
34. Guerra, F.; Arbini, A.A.; Moro, L. Mitochondria and cancer chemoresistance. *Biochim. Biophys. Acta. Bioenerg.* **2017**, 1858, 686-699. DOI: 10.1016/j.bbabio.2017.01.012
35. Lleonart, M.E.; Abad, E.; Graifer, D.; Lyakhovich, A. Reactive oxygen species-mediated autophagy defines the fate of cancer stem cells. *Antioxid. Redox Signal.* **2018**, 28, 1066-1079. DOI: 10.1089/ars.2017.7223
36. Jones, C.L.; Inguva, A.; Jordan, C.T. Targeting energy metabolism in cancer stem cells: progress and challenges in leukemia and solid tumors. *Cell Stem Cell* **2021**, 28, 378-393. DOI: 10.1016/j.stem.2021.02.013
37. Han, X.; Su, R.; Huang, X.; Wang, Y.; Kuang, X.; Zhou, S.; Liu, H. Triphenylphosphonium-modified mitochondria-targeted paclitaxel nanocrystals for overcoming multidrug resistance. *Asian Journal of Pharmaceutical Sciences* **2019**, 14, 569-580. DOI: 10.1016/j.ajps.2018.06.006
38. Lu, A.T.; Quach, A.; Wilson, J.G.; Reiner, A.P.; Aviv, A.; Raj, K.; Hou, L.; Baccarelli, A.A.; Li, Y.; Stewart, J.D.; Whitsel, E.A.; Assimes, T.L.; Ferrucci, L.; Horvath, S. DNA methylation GrimAge strongly predicts lifespan and healthspan. *Aging (Albany N.Y.)* **2019**, 11, 303-327. DOI: 10.18632/aging.101684
39. Liu, H.N.; Guo, N.N.; Wang, T.T.; Guo, W.W.; Lin, M.T.; Huang-Fu, M.Y.; Vakili, M.R.; Xu, W.H.; Chen, J.J.; Wei, Q.C.; Han, M.; Lavasanifar, A.; Gao, JQ. Mitochondrial targeted doxorubicin-triphenylphosphonium delivered by hyaluronic acid modified and ph responsive nanocarriers to breast tumor: *in vitro* and *in vivo* studies. *Mol. Pharm.* **2018**, 15, 882-891. DOI: 10.1021/acs.molpharmaceut.7b00793
40. Ozsvari, B.; Sotgia, F.; Lisanti, M.P. Exploiting mitochondrial targeting signal(s), TPP and bis-TPP, for eradicating cancer stem cells (CSCs). *Aging (Albany N.Y.)* **2018**, 10, 229-240. DOI: 10.18632/aging.101384
41. Kalghatgi, S.; Spina, C.S.; Costello, J.C.; Liesa, M.; Morones-Ramirez, J.R.; Slomovic, S.; Molina, A.; Shirihai, O.S.; Collins, J.J. Bactericidal antibiotics induce mitochondrial dysfunction and oxidative damage in Mammalian cells. *Sci. Transl. Med.* **2013**, 5, 192ra85. DOI: 10.1126/scitranslmed.3006055
42. Lleonart, M.E., Grodzicki, R.; Graifer, D.M.; Lyakhovich, A. Mitochondrial dysfunction and potential anticancer therapy. *Med. Res. Rev.* **2017**, 37, 1275-1298. DOI: 10.1002/med.21459
43. Fiorillo, M.; Lamb, R.; Tanowitz, H.B.; Cappello, A.R.; Martinez-Outschoorn, U.E.; Sotgia, F.; Lisanti, M.P. Bedaquiline, an FDA-approved antibiotic, inhibits mitochondrial function and potently blocks the proliferative expansion of stem-like cancer cells (CSCs). *Aging (Albany N.Y.)* **2016**, 8, 1593-1607. DOI: 10.18632/aging.100983
44. Kuntz, E.M.; Baquero, P.; Michie, A.M.; Dunn, K.; Tardito, S.; Holyoake, T.L.; Helgason, G.V.; Gottlieb, E. Targeting mitochondrial oxidative phosphorylation eradicates therapy-resistant chronic myeloid leukemia stem cells. *Nat. Med.* **2017**, 23, 1234-1240. DOI: 10.1038/nm.4399
45. Nissen, P.; Hansen, J.; Ban, N.; Moore, P.B.; Steitz, T.A. The structural basis of ribosome activity in peptide bond synthesis. *Science* **2000**, 289, 920-930. DOI: 10.1126/science.289.5481.920
46. Contreras, A.; Vazquez, D. Cooperative and antagonistic interactions of peptidyl-tRNA and antibiotics with bacterial ribosomes. *Eur. J. Biochem.* **1977**, 74, 539–547. DOI: 10.1111/j.1432-1033.1977.tb11422.x
47. Dinos, G.P.; Athanassopoulos, C.M.; Missiri, D.A.; Giannopoulou, P.C.; Vlachogiannis, I.A.; Papadopoulos, G.E.; Papaioannou, D.; Kalpaxis, D.L. Chloramphenicol derivatives as antibacterial and anticancer agents: historic problems and current solutions. *Antibiotics (Basel)* **2016**, 5, 20. DOI: 10.3390/antibiotics5020020
48. Tereshchenkov, A.G.; Dobosz-Bartoszek, M.; Osterman, I.A.; Marks, J.; Sergeeva, V.A.; Kasatsky, P.; Komarova, E.S.; Stavrianidi, A.N.; Rodin, I.A.; Konevega, A.L.; Sergiev, P.V.; Sumbatyan, N.V.; Mankin, A.S.; Bogdanov, A.A.; Polikanov, Y.S. Binding and action of amino acid analogs of chloramphenicol upon the bacterial ribosome. *J Mol Biol.* **2018**, 430, 842-852. DOI: 10.1016/j.jmb.2018.01.016
49. Mamos, P.; Krokidis, M.G.; Papadas, A.; Karahalios, P.; Starosta, A.L.; Wilson, D.N.; Kalpaxis, D.L.; Dinos, G.P. On the use of the antibiotic chloramphenicol to target polypeptide chain mimics to the ribosomal exit tunnel. *Biochimie* **2013**, 95, 1765-72. DOI: 10.1016/j.biochi.2013.06.004
50. Kostopoulou, O.N.; Kouvela, E.C.; Magoulas, G.E.; Garnelis, T.; Panagoulias, I.; Rodi, M.; Papadopoulos, G.; Mouzaki, A.; Dinos, G.P.; Papaioannou, D.; Kalpaxis, D.L. Conjugation with polyamines enhances the antibacterial and anticancer activity of chloramphenicol. *Nucleic Acids Res.* **2014**, 42, 8621-34. DOI: 10.1093/nar/gku539
51. Giannopoulou, P.C.; Missiri, D.A.; Kournoutou, G.G.; Sazakli, E.; Papadopoulos, G.E.; Papaioannou, D.; Dinos, G.P.; Athanassopoulos, C.M.; Kalpaxis, D.L. New Chloramphenicol Derivatives from the Viewpoint of Anticancer and Antimicrobial Activity. *Antibiotics* **2019**, 8, 9. DOI: 10.3390/antibiotics8010009
52. Yan, K.; Hunt, E.; Berge, J.; May, E.; Copeland, R.A.; Gontarek, R.R. Fluorescence polarization method to characterize macrolide-ribosome interactions. *Antimicrob. Agents Chemother.* **2005**, 49, 3367-3372. DOI: 10.1128/AAC.49.8.3367-3372.2005
53. Tereshchenkov, A.G.; Shishkina, A.V.; Tashlitsky, V.N.; Korshunova, G.A.; Bogdanov, A.A.; Sumbatyan, N.V. Interaction of chloramphenicol tripeptide analogs with ribosomes. *Biochemistry (Moscow, Russ. Fed.)* **2016**, 81, 392-400. DOI: 10.1134/S000629791604009X
54. Osterman, I.A.; Komarova, E.S.; Shiryaev, D.I.; Korniltsev, I.A.; Khven, I.M.; Lukyanov, D.A.; Tashlitsky, V.N.; Serebryakova, M.V.; Efremenkova, O.V.; Ivanenkov, Y.A.; Bogdanov, A.A.; Sergiev, P.V.; Dontsova, O.A. Sorting out antibiotics'

mechanisms of action: a double fluorescent protein reporter for high-throughput screening of ribosome and DNA biosynthesis inhibitors. *Antimicrob Agents Chemother* **2016**, 60, 7481-7489. DOI: 10.1128/AAC.02117-16

55. Rebstock, M.C.; Crooks, H.M.; Controulis, J.; Bartz, Q.R. Chloramphenicol (chloromycetin). IV. Chemical studies. *J. Am. Chem. Soc.* **1949**, 71, 2458–2462. DOI: 10.1021/ja01175a065
56. Marks, J.; Kannan, K.; Roncase, E.J.; Klepacki, D.; Kefi, A.; Orelle, C.; Vázquez-Laslop, N.; Mankin, A.S. Context-specific inhibition of translation by ribosomal antibiotics targeting the peptidyl transferase center. *Proc Natl Acad Sci USA* **2016**, 113, 12150-12155. DOI: 10.1073/pnas.1613055113
57. Hartz, D.; McPheeters, D.S.; Traut, R.; Gold, L. Extension inhibition analysis of translation initiation complexes. *Methods Enzymol.* **1988**, 164, 419-425. DOI: 10.1016/s0076-6879(88)64058-4
58. Makarova, T.M. 2020. Investigation of allosteric phenomena in the bacterial ribosome by molecular dynamics simulations method, Ph.D. dissertation, Lomonosov Moscow State University, Moscow, Russia, September 21.
59. Makarov, G.I.; Makarova, T.M. A noncanonical binding site of chloramphenicol revealed via molecular dynamics simulations. *Biochim. Biophys. Acta, Gen. Subj.* **2018**, 1862, 2940-2947. DOI: 10.1016/j.bbagen.2018.09.012
60. Nazarov, P.A.; Kotova, E.A.; Skulachev, V.P.; Antonenko, Y.N. Genetic variability of the AcrAB-TolC multidrug efflux pump underlies SkQ1 resistance in gram-negative bacteria. *Acta Naturae.* **2019**, 11, 93-98. DOI: 10.32607/20758251-2019-11-4-93-98
61. Long, K.S.; Poehlsgaard, J.; Kehrenberg, C.; Schwarz, S.; Vester, B. The Cfr rRNA methyl-transferase confers resistance to phenicols, lincosamides, oxazolidinones, pleuromutilins, and streptogramin A antibiotics. *Antimicrob Agents Chemother* **2006**, 50, 2500-2505. DOI: 10.1128/AAC.00131-06
62. Mosmann, T. Rapid colorimetric assay for cellular growth and survival: application to proliferation and cytotoxicity assays. *J Immunol Methods* **1983**, 65, 55-63. DOI: 10.1016/0022-1759(83)90303-4
63. Antonenko, Y.N.; Avetisyan, A.V.; Bakeeva, L.E.; Chernyak, B.V.; Chertkov, V.A.; Domnina, L.V.; Ivanova, O.Y.; Izyumov, D.S.; Khailova, L.S.; Klishin, S.S.; Korshunova, G.A.; Lyamzaev, K.G.; Muntyan. M.S.; Nepryakhina, O.K.; Pashkovskaya, A.A.; Pletjushkina, O.Y.; Pustovidko, A.V.; Roginsky, V.A.; Rokitskaya, T.I.; Ruuge, E.K.; Saprunova, V.B.; Severina, I.I.; Simonyan, R.A.; Skulachev, I.V.; Skulachev, M.V.; Sumbatyan, N.V.; Sviryaeva, I.V.; Tashlitsky, V.N.; Vassiliev, J.M.; Vyssokikh, M.Y.; Yaguzhinsky, L.S.; Zamyatnin Jr., A.A.; Skulachev, V.P. Mitochondria-targeted plastoquinone derivatives as tools to interrupt execution of the aging program. 1. Cationic plastoquinone derivatives: synthesis and *in vitro* studies. *Biochemistry (Moscow, Russ. Fed.)* **2008**, 73, 1273-1287. DOI: 10.1134/s0006297908120018
64. Ross, M.F.; Prime, T.A.; Abakumova, I.; James, A.M.; Porteous, C.M.; Smith, R.A.; Murphy, M.P. Rapid and extensive uptake and activation of hydrophobic triphenylphosphonium cations within cells. *Biochem. J.* **2008**, 411, 633-645. DOI: 10.1042/BJ20080063
65. Neuzil, J.; Dong, L.F.; Rohlena, J.; Truksa, J.; Ralph, S.J. Classification of mitocans, anti-cancer drugs acting on mitochondria. *Mitochondrion* **2013**, 13, 199-208. DOI: 10.1016/j.mito.2012.07.112
66. Ralph, S.J.; Low, P.; Dong, L.; Lawen, A.; Neuzil, J. Mitocans: mitochondrial targeted anti-cancer drugs as improved therapies and related patent documents. *Recent Pat. Anticancer Drug Discov.* **2006**, 1, 327-346. DOI: 10.2174/157489206778776952
67. Abad, E.; García-Mayea, Y.; Mir, C.; Sebastian, D.; Zorzano, A.; Potesil, D.; Zdrahal, Z.; Lyakhovich, A.; Lleonart, M.E. Common metabolic pathways implicated in resistance to chemotherapy point to a key mitochondrial role in breast cancer. *Mol. cell proteomics* **2019**, 18, 231-244. DOI: 10.1074/mcp.RA118.001102
68. Esner, M.; Graifer, D.; Lleonart, M.E.; Lyakhovich, A. Targeting cancer cells through antibiotics-induced mitochondrial dysfunction requires autophagy inhibition. *Cancer Lett.* **2017**, 384, 60-69. DOI: 10.1016/j.canlet.2016.09.023
69. Shishkina, A.V.; Makarov, G.I.; Tereshchenkov, A.G.; Korshunova, G.A.; Sumbatyan, N.V.; Golovin, A.V.; Svetlov, M.S.; Bogdanov, A.A. Conjugates of amino acids and peptides with 5-o-mycaminosyltylonolide and their interaction with the ribosomal exit tunnel. *Bioconjug Chem.* **2013**, 24, 1861-1869. DOI: 10.1021/bc400236n
70. Wang, Z.X. An exact mathematical expression for describing competitive binding of two different ligands to a protein molecule. *FEBS Lett*. **1995,** 360, 111-114. DOI: 10.1016/0014-5793(95)00062-e
71. Baba, T.; Ara, T.; Hasegawa, M.; Takai, Y.; Okumura, Y.; Baba, M.; Datsenko, K.A.; Tomita, M.; Wanner, B.L.; Mori, H. Construction of *Escherichia coli* K-12 in-frame, single-gene knockout mutants: the Keio collection. *Mol Syst Biol*. **2006**, 2. DOI: 10.1038/msb4100050
72. Zakalyukina, Y.V.; Birykov, M.V.; Lukianov, D.A.; Shiriaev, D.I.; Komarova, E.S.; Skvortsov, D.A.; Kostyukevich, Y.; Tashlitsky, V.N.; Polshakov, V.I.; Nikolaev, E.; Sergiev, P.V.; Osterman, I.A. Nybomycin-producing *Streptomyces* isolated from carpenter ant *Camponotus vagus*. *Biochimie* **2019,** 160, 93-99. DOI: 10.1016/j.biochi.2019.02.010
73. Orelle, C.; Szal, T.; Klepacki, D.; Shaw, K.J.; Vázquez-Laslop, N.; Mankin, A.S. Identifying the targets of aminoacyl-tRNA synthetase inhibitors by primer extension inhibition. *Nucleic Acids Res.* **2013**, 41, e144. DOI: 10.1093/nar/gkt526
74. Cao, G.; Zhang, X.; Zhong, L.; Lu, Z. A modified electro-transformation method for *Bacillus subtilis* and its application in the production of antimicrobial lipopeptides. *Biotechnol Lett*. **2011**, 33, 1047-1051. DOI: 10.1007/s10529-011-0531-x
75. Lu, Y.P.; Zhang, C.; Lv, F.X.; Bie, X.M.; Lu, Z.X. Study on the electro-transformation conditions of improving transformation efficiency for *Bacillus subtilis*. *Lett Appl Microbiol*. **2012**, 55, 9-14. DOI: 10.1111/j.1472-765X.2012.03249.x
76. Antonenko, Y.N.; Denisov, S.S.; Khailova, L.S.; Nazarov, P.A.; Rokitskaya, T.; Tashlitsky, V.N.; Firsov, A.M.; Korshunova, G.A.; Kotova, E.A. Alkyl-substituted phenylamino derivatives of 7-nitrobenz-2-oxa-1,3-diazole as uncouplers of oxidative phosphorylation and antibacterial agents: involvement of membrane proteins in the uncoupling action. *Biochim Biophys Acta Biomembr*. **2017**, 1859, 377-387. DOI: 10.1016/j.bbamem.2016.12.014

77. Abad, E.; Civit, L.; Potesil, D.; Zdrahal, Z.; Lyakhovich, A. Enhanced DNA damage response through RAD50 in triple negative breast cancer resistant and cancer stem-like cells contributes to chemoresistance. *FEBS J.* **2020**. DOI: 10.1111/febs.15588
78. Makarov, G. I.; Makarova, T. M. A noncanonical binding site of linezolid revealed via molecular dynamics simulations. *Journal of Computer-Aided Molecular Design* **2019**, 34, 281–291. DOI:10.1007/s10822-019-00269-x
79. Schlünzen, F.; Zarivach, R.; Harms, J.; Bashan, A.; Tocilj, A.; Albrecht, R.; Yonath, A.; Franceschi, F. Structural basis for the interaction of antibiotics with the peptidyl transferase centre in eubacteria. *Nature* **2001,** 413, 814-821. DOI: 10.1038/35101544
80. Ruiz-Carmona, S.; Alvarez-Garcia, D.; Foloppe, N.; Garmendia-Doval, A. B.; Juhos, S.; Schmidtke, P.; Barril, X.; Hubbard, R. E.; Morley, S. D. rDock: A fast, versatile and open source program for docking ligands to proteins and nucleic acids. *PLoS Comput Biol* **2014**, 10, e1003571. DOI: 10.1371/journal.pcbi.1003571
81. Hess, B.; Bekker, H.; Berendsen, H.J.C.; Fraaije, J.G.E.M. LINCS: A linear constraint solver for molecular simulations. *J. Comput. Chem.* **1997**, 18, 1463–1472. DOI: 10.1002/(SICI)1096-987X(199709)18:12<1463::AID-JCC4>3.0.CO;2-H
82. Bussi, G.; Donadio, D.; Parrinello, M. Canonical sampling through velocity rescaling. *J Chem Phys*. **2007**, 126, 014101-014102. DOI: 10.1063/1.2408420
83. Berendsen, H.J.C.; Postma, J.P.M.; van Gunsteren, W.F.; DiNola, A.; Haak, J.R. Molecular dynamics with coupling to an external bath. *The Journal of Chemical Physics* **1984,** 81, 3684–3690. DOI: 10.1063/1.448118
84. Darden, T.; York, D.; Pedersen, L. Particle mesh Ewald: AnN·log(N) method for Ewald sums in large systems. *The Journal of Chemical Physics* **1993,** 98, 10089–10092. 10.1063/1.464397
85. Horn, H.W.; Swope, W.C.; Pitera, J.W.; Madura, J.D.; Dick, T.J.; Hura, G.L.; Head-Gordon, T. Development of an improved four-site water model for biomolecular simulations: TIP4P-Ew. *J Chem Phys*. **2004**, 120, 9665-9678. DOI: 10.1063/1.1683075
86. Athavale, S.S.; Petrov, A.S.; Hsiao, C.; Watkins, D.; Prickett, C.D.; Gossett, J.J.; Lie, L.; Bowman, J.C.; O'Neill, E.; Bernier, C.R.; Hud, N.V.; Wartell, R.M.; Harvey, S.C.; Williams, L.D. RNA folding and catalysis mediated by iron (II). *PLoS One*. **2012**, 7, e38024. DOI: 10.1371/journal.pone.0038024
87. Hornak, V.; Abel, R.; Okur, A.; Strockbine, B.; Roitberg, A.; Simmerling, C. Comparison of multiple Amber force fields and development of improved protein backbone parameters. *Proteins*. **2006**, 65, 712-25. DOI: 10.1002/prot.21123
88. Wang, J.; Wolf, R.M.; Caldwell, J.W.; Kollman, P.A.; Case, D.A. Development and testing of a general amber force field. *J. Comput. Chem*. **2004**, 25: 1157–1174. DOI: 10.1002/jcc.20035
89. Bayly, C.I.; Cieplak, P.; Cornell, W.; Kollman, P.A. A well-behaved electrostatic potential based method using charge restraints for deriving atomic charges: the RESP model. *J Phys Chem* **1993,** 97, 10269–10280. DOI: 10.1021/j100142a004
90. Van der Spoel, D.; Lindahl, E.; Hess, B.; Groenhof, G.; Mark, A.E.; Berendsen, H.J. GROMACS: fast, flexible, and free. *J Comput Chem.* **2005**, 26, 1701-1718. DOI: 10.1002/jcc.20291
91. Hess, B.; Kutzner, C.; van der Spoel, D.; Lindahl, E. GROMACS 4: Algorithms for highly efficient, load-balanced, and scalable molecular simulation. *J Chem Theory Comput*. **2008**, 4, 435-447. DOI: 10.1021/ct700301q
92. Makarov, G.I.; Sumbatyan, N.V.; Bogdanov, A.A. Structural insight into interaction between C20 phenylalanyl derivative of tylosin and ribosomal tunnel. *Biochemistry (Mosc).* **2017**, 82, 925-932. DOI: 10.1134/S0006297917080077
93. Daura, X.; Gademann, K.; Jaun, B.; Seebach, D.; van Gunsteren, W.F.; Mark, A.E. Peptide folding: when simulation meets experiment. *Angew Chem Int Ed* **1999,** 38, 236–240. DOI: 10.1002/(SICI)1521-3773(19990115)38:1/2<236::AID-ANIE236>3.0.CO;2-M